

Crustal features of the northeastern South China Sea: insights from seismic and magnetic interpretations

Yi-Ching Yeh · Shu-Kun Hsu · Wen-Bin Doo ·
Jean-Claude Sibuet · Char-Shine Liu ·
Chao-Shing Lee

Received: 30 September 2011 / Accepted: 2 May 2012 / Published online: 29 May 2012
© Springer Science+Business Media B.V. 2012

Abstract We interpret seven two-dimensional deep-penetration and long-offset multi-channel seismic profiles in the northernmost South China Sea area, which were collected by *R/V Marcus G. Langseth* during the TAIwan GEodynamics Research (TAIGER) project in 2009. To constrain the crustal characteristics, magnetic inversion and forward magnetic modeling were also performed. The seismic results clearly show tilted faulting blocks in the upper crust and most of the fault plane connects downward to a quasi-horizontal detachment as its bottom in the south of the Luzon-Ryukyu transform plate boundary. North of the plate boundary, a small-scale failed rifted basin (minimum 5 km in crustal thickness) with negative magnetization probably indicates an extended continental origin. Significant lower crustal material (LCM) was imaged under a crustal fracture area which indicated a continent and ocean transition origin. The thickest LCM (up to 6.5 km) is located at magnetic isochron C15 that is probably caused by the magma supply composite of a Miocene syn-rift volcanic event and Pliocene Dongsha volcanic activity for submarine volcanoes and sills in the surrounding area. The LCM also caused Miocene crustal blocks to be uplifted reversely as 17 km crustal thickness

especially in the area of magnetic isochron C15 and C16. In addition, the wide fault blocks and LCM co-existed on the magnetic striped area (i.e. C15–C17) in the south of the Luzon-Ryukyu transform plate boundary. Magnetic forward modeling suggests that the whole thick crustal thickness (>12 km thick) needs to be magnetized in striped way as oceanic crust. However, the result also shows that the misfit between observed and synthetic magnetic anomaly is about 40 nT, north of isochron C16. The interval velocity derived from pre-stack time migration suggests that the crust is composed of basaltic intrusive upper crust and lower crustal material. The crustal nature should refer to a transition between continent and ocean. Thus, the magnetic reversals may be produced in two possible ways: basaltic magma injected along the crustal weak zone across magnetic reversal epoch and because some undiscovered ancient piece of oceanic crust existed. The crustal structure discrimination still needs to be confirmed by future studies.

Keywords Crustal structures · Passive margin · Pre-stack time migration · Magnetization · Northern South China Sea · TAIGER project

Y.-C. Yeh (✉) · C.-S. Lee
Institute of Applied Geosciences, National Taiwan Ocean University, 2 Beining Road, Keelung 20224, Taiwan
e-mail: yiching.yeh@gmail.com

S.-K. Hsu · W.-B. Doo · J.-C. Sibuet
Institute of Geophysics, National Central University,
300 Chungda Road, Jhongli 32001, Taiwan

C.-S. Liu
Institute of Oceanography, National Taiwan University,
1, Sec.4 Roosevelt Road, Taipei 10617, Taiwan

Introduction

Passive continental margins can be divided into two categories: volcanic (magma-rich) and non-volcanic (magma-poor) on the basis of the volume of magma supply during continental crust break-up (Louden and Chian 1999; Menzies et al. 2002). The main character of a magma-rich margin is that a large volume of basalt erupted during the early stage of the continental crust break-up. Because of duplicated basaltic magma during initial oceanic crust creation, seaward dipping reflectors (SDRs) are commonly

imaged within the upper crust. Additionally, in the syn-rift to post-rift stage, lower crustal magmatism (underplating) often appears in continent-ocean transitions such as the Vøring margin (Mjelde et al. 2002; Voss and Jokat 2007). Conversely, at magma-poor margins, only volcanic intrusion/extrusion form as sills (e.g. the U reflector in the Newfoundland margin; Péron-Pinvidic et al. 2010). Wide continent-to-ocean transition zones with numerous tilted crustal blocks often appear. The most remarkable feature is the mantle exhumation that normally creates a peridotite ridge regarded as the boundary between oceanic and continental crust as shown in the Iberia margin (Sibuet et al. 2007; Tucholke et al. 2007; Sibuet and Tucholke 2012). Moreover, the lower continental crust will be exhumed then exposed to the seafloor when the lower crust is ductile, as in the Angola/Congo margin. In addition, Clift et al. (2001) also suggested there is a very weak lower crust layer in the northwestern South China Sea (SCS) margin during continental breakup. However, unlike the typical magma-poor or magma-rich margin, there is no obvious evidence for the initial stage of basaltic magma deposition (SDRs) or mantle exhumation (peridotite ridge) in the continent–ocean transition area of the SCS.

The northern SCS continental margin was rifted since Cretaceous time, then the breakup of the SCS at late Eocene time, followed by oceanic crust creation (Ru and Pigott 1986; Ren et al. 2002). Based on latest magnetic studies in the middle to northernmost SCS, the oceanic crust could be extended to the offshore area of southwestern Taiwan (Hsu et al. 2004; Yeh et al. 2010). The oldest oceanic crust identified could be as old as 37.8 Ma, corresponding to magnetic isochron C17 (Hsu et al. 2004). However, relatively thick (10–12 km) crust was also identified by forward gravity modeling (Tsai et al. 2004; Yeh and Hsu 2004). In the upper crust, post-rifting extensional tectonic activity was recorded as tilted crustal blocks (Yeh et al. 2010). This crustal structure could be interpreted as either a thinned continental crust with magmatic intrusion or thick oceanic crust with volcanic intrusion (Nissen et al. 1995; Kido et al. 2001; Yeh et al. 2010). Furthermore, one wide-angle refraction profile (Wang et al. 2006) in this area shows the existence of lower crust material. An S-wave tomography study of the same ocean-bottom seismometer (OBS) profile indicated a V_p/V_s 1.76–1.94 for lower crustal material (LCM), implying a mafic composition (Zhao et al. 2010). The LCM will attach to the lower crust of the rifted continental crust at the continental–oceanic transition area especially in volcanic margins (Gernigon et al. 2006). The large-volume basaltic eruptions will overlie above the rifted continental crust then form seaward-dipping reflectors in seismic investigation. However, the interbedded highly reflective layer as sills caused by magma injection is also typically

characteristic of the volcanic margin (Berndt et al. 2000; Svensen et al. 2004). Therefore, the crustal nature of northern SCS could be classified as rifted continental crust with magmatic underplating. However, this interpretation conflicts with the magnetic results that suggested northern SCS should be thick oceanic domain caused by post-spreading volcanism (Hsu et al. 2004). Hsu et al. (2004) interpreted that an oceanic domain (i.e. magnetic isochron C15–C17) was characterized by post-spreading volcanism. Several N–S trending magnetic anomalies low in between magnetic reversals were suggested to be oceanic fracture zones. In summary, the thick oceanic crust model is very different from the thinned continental crust model. The different crustal nature interpretations will also affect our knowledge of the northern SCS margin in evolutionary and dynamical points of view. In this study, we first present whole crustal images (i.e. to Moho interface) of seven multichannel seismic profiles in the northeastern SCS area, and analyze them to attempt to resolve the disparate interpretations of SCS crustal composition discussed above. The seismic data were collected by the marine TAIwan Integrated GEodynamics Research (TAIGER) project in 2009. In addition, we performed a magnetic inversion and forward magnetic modeling to discuss the possible crustal characteristics.

Tectonic settings of the northeastern South China Sea

Two main kinematic models have been proposed for the seafloor spreading evolution of the SCS. The first model was proposed by Taylor and Hayes (1980, 1983). They identified the oldest seafloor spreading magnetic lineation as C11 (i.e. ~32 Ma). They proposed that the SCS margin began rifted in the early Miocene and the following seafloor spreading was driven both by right-lateral shear along the offshore Vietnam transform fault, with Indochina and Borneo fixed relative to South China and subduction of the proto-SCS slab beneath Palawan. Briais et al. (1993) analyzed Chinese Atlas magnetic data (Chen 1987) and similarly suggested the SCS started spreading at isochron C12 (~32 Ma) and ceased at C5c (~16.5 Ma) with two to three staged ridge jumps. The main driving force of the SCS was the left-lateral shear movement of the Red River–Ailaoshan fault zone at late Eocene. Nevertheless, Barckhausen and Roeser (2004) pointed out the cessation of the seafloor spreading should be as old as 20.5 Ma, earlier than in other models, by using the data collecting in the southwestern SCS subbasin. Any age model presented by several groups in past decades has had insufficient data in the northeastern corner of the SCS. In contrast, the three pairs of magnetic reversals in the north of magnetic isochron C12 (CCOP 1994; Hsu et al. 2004) strongly imply

the existence of older oceanic crust off southwest Taiwan (Hsu et al. 2004). The oldest seafloor spreading episode of the SCS was therefore identified as late Eocene (Hsu et al. 2004). A combined analysis of all the available marine geophysical data (i.e. swath-bathymetry, magnetic, gravity and MCS), a new kinematic framework for northern SCS was presented by Yeh et al. (2010). They demonstrated that the SCS started to rift in a complex way and went through four spreading direction changes with several fracture zones. Two post-rifting unconformities were clearly identified, which indicates post-rift extension and magmatic intrusion at 30 and 22 Ma, respectively. In addition, a Pliocene Dongsha uplift (~ 5.2 Ma) caused by magma intrusions (Lüdmann and Wong 1999) which reactivated the pre-existing Miocene basement blocks related to SCS opening in the southwestern study area (Fig. 1). Thus, three unconformities were recorded in the stratigraphic column. Besides, all the seafloor spreading features were limited to the south of the Luzon-Ryuku plate boundary (Yeh et al. 2010), which is a proposed transform plate boundary (Fig. 1) between the SCS oceanic terrane and another unnamed oceanic terrane identified by free-air gravity and magnetic data (Sibuet et al. 2002; Hsu et al. 2004; Li et al. 2007). However, the basement topography shows that it gradually dips to the north due to differential post-rift subsidence. The forward gravity modeling result also shows a slight difference of the crustal thickness. The obvious crustal shear (composite extension and uplifting) deformation was imaged only near the northwest and southeast ends of the Luzon-Ryuku transform plate boundary (Yeh and Hsu 2004). This is probably related to different oceanic terrane subduction (proto-SCS or unknown oceanic terrane) or due to post-spreading magmatism imprinting on the pre-existing SCS crusts (Hsu et al. 2004).

Multichannel seismic data acquisition and processing

To understand the tectonic and geodynamic processes of the Taiwan orogeny and surrounding area, two-dimensional long-offset multichannel seismic (MCS) data were collected in the northern South China Sea and Western Philippine Sea regions from April to July 2009 during three TAIGER project research cruises (MGL0905, MGL0906 and MGL0908) using R/V *Marcus G. Langseth*. Figure 1 shows the locations of the MCS data used in this study. A 6,000 meter 468-channel hydrophone streamer with a 12.5 m group spacing was used to record a 6,600-cubic-inch source array consisting of four stream mixed air guns and G–I (generator–injector) guns. The shot interval was fixed at 50 meters, controlled by differential global positioning system resulting in a minimum of 60-fold CMP

data. The recording length was 15 s with a 2-millisecond (ms) sampling interval.

The data were re-sampled to a 4-ms sample interval. We then applied geometry setting, trace editing, semblance stacking velocity picking and amplitude correction for spherical divergence ($1/(t \times V^2)$) using stacking velocity. We then produced initial stacked sections which determined the quality of velocity picking. Multiple attenuation was then applied by either F–K multiple attenuation, Radon Transform multiple suppression or surface related wave equation multiple attenuation (SRME) based on source structures of the multiple occurrences (i.e. seafloor relief or complexity of structures). Once the de-multiple procedure was finished, post-stack Kirchhoff time migration (Yilmaz 2008) produced the time migration sections for comparison and quality control. Considering the relatively high lateral velocity variation and structural complexity (continental–oceanic crust transition) in the study area, we also applied pre-stack time migration. The stacking velocity table was converted to internal velocity to form the initial velocity model. By using a layer-stripping approach, the velocity was updated and modified from the seafloor down to the Mohorovičić Discontinuity (Moho). In each iteration step, we compared the pre-stack Kirchhoff time migration (PSTM) section to the post-stack section to avoid migration artifact. After six iterations of velocity updates, the final pre-stack time migration sections were produced. Finally, a time variant band pass filter (i.e. upper bound is 10–20–64–128 Hz; lower bound is 3–16–32–64 Hz) and post migration F–K filter were applied, before producing the final images (Figs. 2, 3, 4, 5, 6, 7, 8). The final rms velocity from PSTM processing was converted to interval velocity by using the Dix formula (Dix 1952) then illustrated crustal thickness and lower-crustal thickness maps in kilometers. The results are shown in Figs. 9 and 10.

Magnetic inversion

To compare the seismic and magnetic characteristics of the crust in the northeastern SCS, we performed a magnetization inversion. The inclination and declination were assumed to be the same as the present day. The IAGF 11 model (IAGA 2010) indicates the inclination and declination are 31.92° and -2.93° , respectively. The latest marine magnetic anomaly map in the study area was compiled by National Central University group, Taiwan (S–K Hsu 2011 personal communication). The magnetic anomaly data was re-gridded into 4 km \times 4 km. A 4 km \times 4 km horizontal model block was set for minimizing the least-square errors between observed and calculated magnetic anomaly in LSQR algorithm (Paige and Saunders 1982). The top of the magnetized layer was set to be the acoustic basement relief

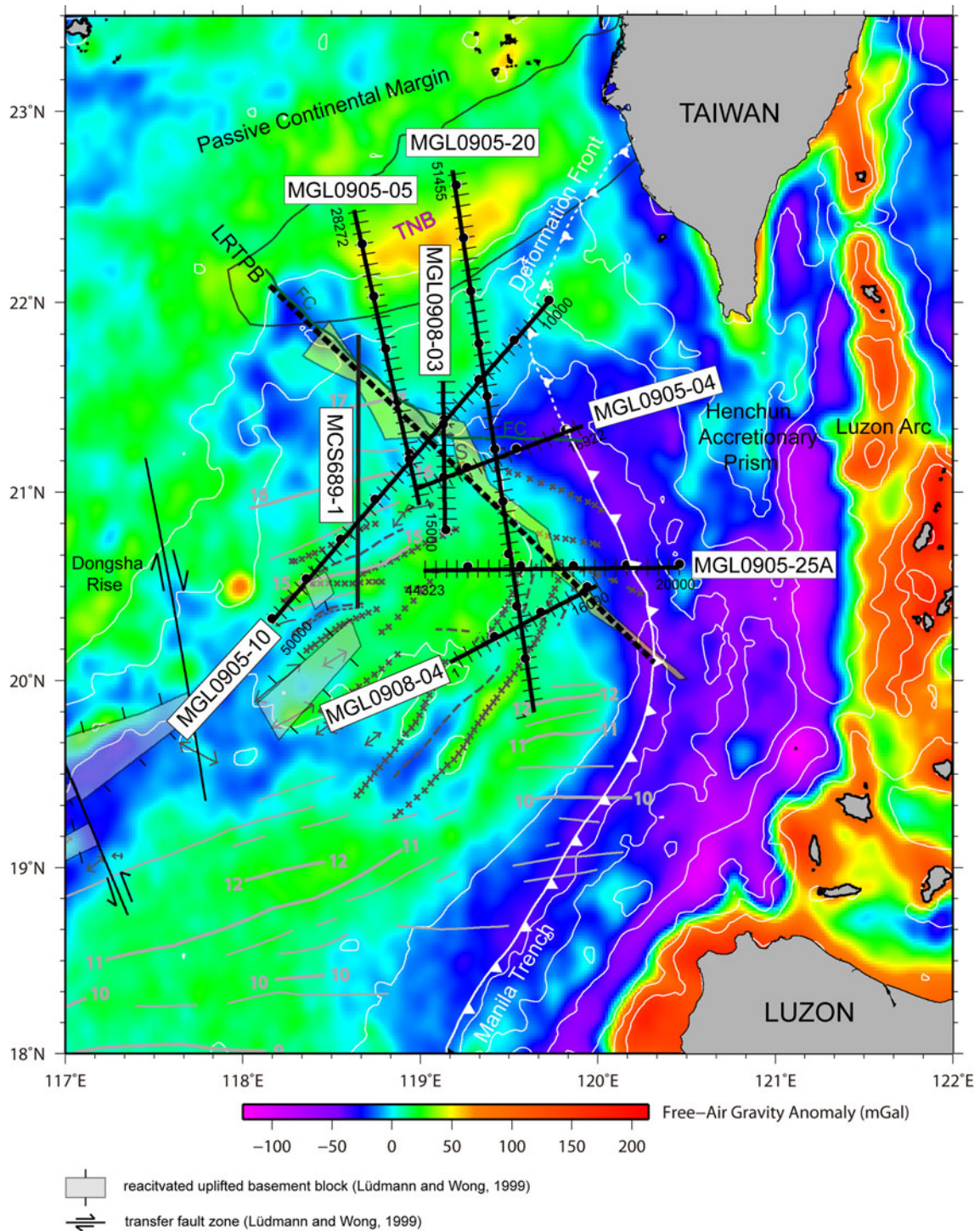


Fig. 1 Satellite-derived free-air gravity anomaly (Sandwell and Smith 1997) draped on swath bathymetry in the study area. Note that the reactivated continental basement blocks (Lüdmann and Wong 1999) correspond to magnetic isochron C15. Black lines are track lines that are used in this study. Dashed line simplified Luzon-Ryukyu transform plate boundary (LRTPB); transparent light yellow area apparent plate boundary area identified by multichannel seismic

interpretations (Yeh et al. 2010); dark grey lines and symbols tectonic interpretations adopted by Yeh et al. (2010); light grey lines and numbers magnetic lineations and isochron by Yeh et al. (2010); small numbers CMP number; bold circle every 5000 CMP; thin line every 200 CMP. The bathymetric contour interval is 200 meters. TNB Tainan Basin

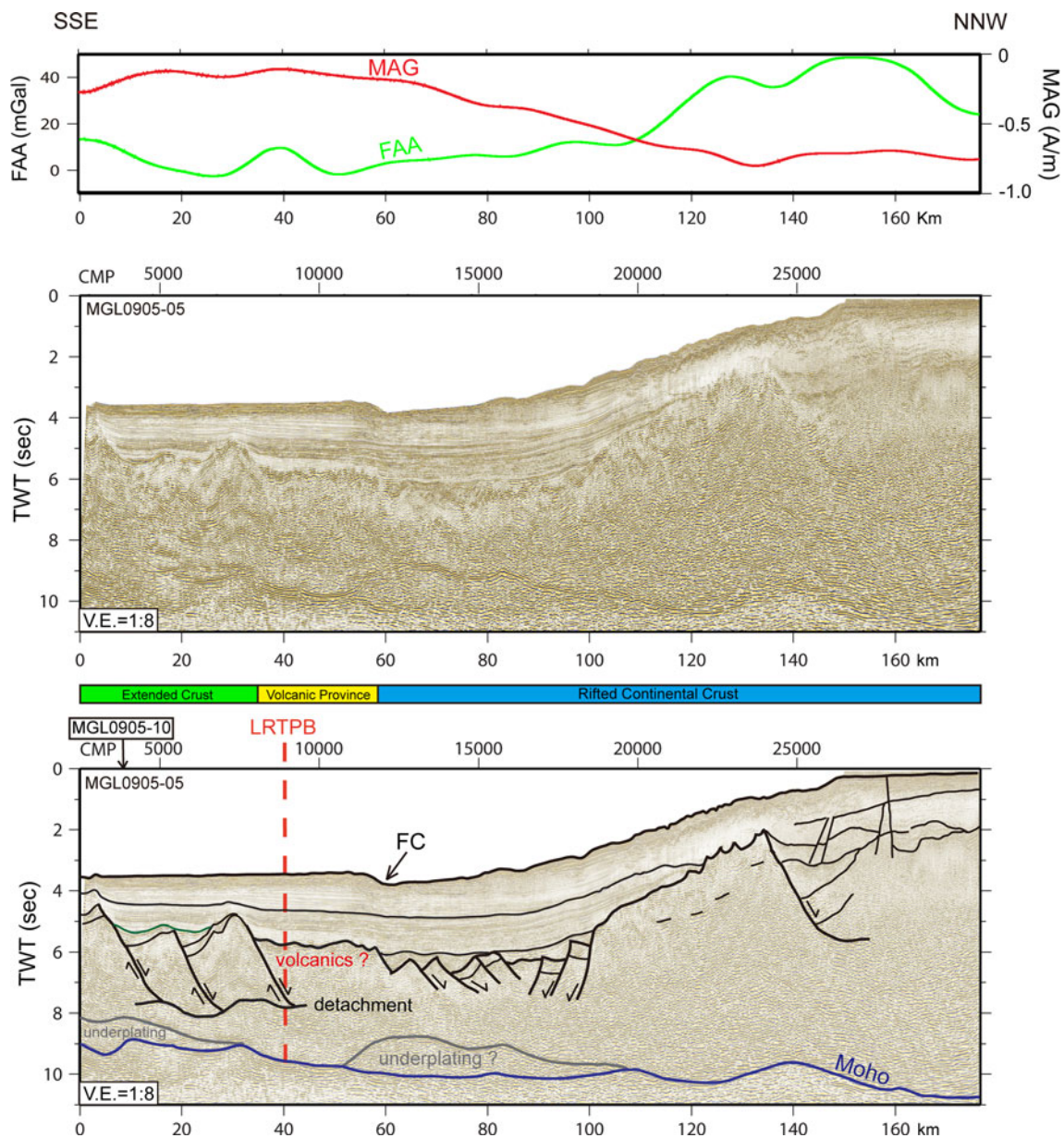


Fig. 2 Pre-stack migration seismic section (PSTM) and its seismic interpretations of line MGL0905-05. At the top of the figure is free-air gravity anomaly and inverted magnetization (Fig. 11). Note that the tilted blocks dip northward south of CMP 10000. A rifting basin is located between CMP 12500 and CMP 19000. North of CMP 24000, the tectonic environment changes to typical passive rifted margin. In addition, there is no Moho depth difference under the Luzon-Ryukyu

transform plate boundary (LRTPB). *Dark green layer* extensional unconformity T1 (Yeh et al. 2010); *grey bold line* top of underplating body; *thin black line* detachment; *bold black line* acoustic basement; *solid red line* sills; *blue line* Moho relief; *thin vertical line* normal fault. *CMP* common mid-point number, *FAA* free-air gravity anomaly, *MAG* magnetization, *FC* Formosa Canyon

and bottom was fixed to 12 km (Wang et al. 2006) in depth (e.g. we refer to the seismic interpretation of line MGL0905-10). The result is shown in Fig. 11.

Seismic structural interpretations

We present seven MCS profiles in the study area. The PSTM sections and their structural interpretations are

described below. For convenience, each profile is shown in order from west to east. It is noted that several profiles are close to or cut across a magnetization low area which may represent basement fault blocks or transfer fault zones.

LINE MGL0905-05 (Fig. 2)

This profile starts from the northern SCS continental shelf and stops near 2,000 m water depth. Figure 2 shows a

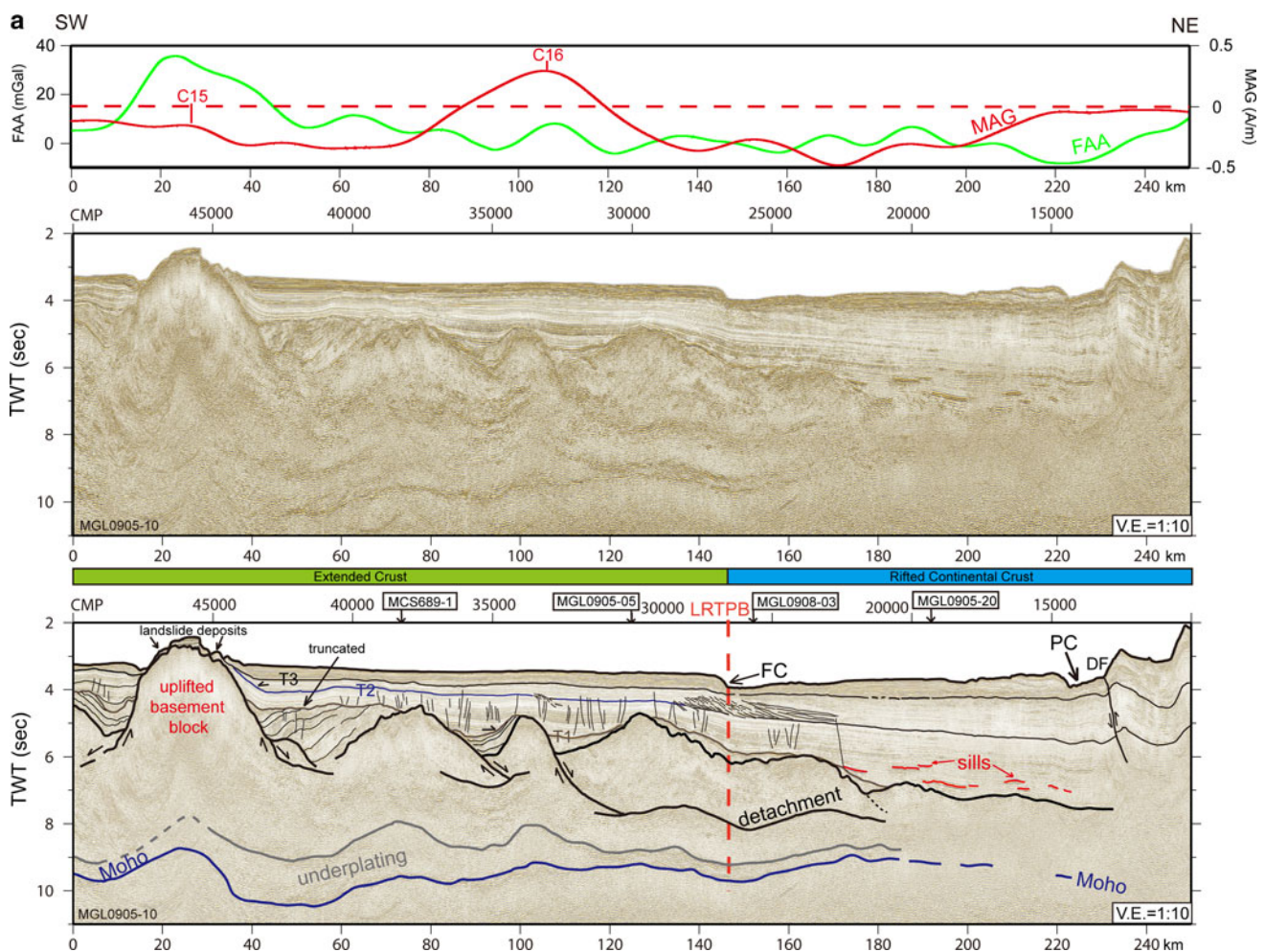


Fig. 3 **a** PSTM section of line MGL0905-10 and its seismic interpretations. **b** MCS689-1 seismic section and its interpretation. Note that the MCS689-1 profile is perpendicular to magnetic lineation C15-C17. The T1 unconformity is also tilted, which marks the relative uplift of basement. The T3 unconformity may correspond to the Pliocene Dongsha uplift event. The relative magnetization is low but acts as magnetic reversals between CMP 46000 and CMP 27500.

PSTM section and its interpretation as well as the corresponding magnetization (i.e. Fig. 11) and free-air gravity anomaly. Starting from the south, the basement was stretched by normal faulting accompanied by syn-rift sediments. The overlapping sediments onlap onto a syn-rift sedimentary sequence that developed an unconformity called T1. This unconformity was identified by Yeh et al. (2010) and dated to 29 Ma. Between CMP numbers 1 and 9000, basement blocks dip 45° landward (northward). The bottoms of the fault planes connect downwards with a detachment of a continuous reflector existing between 7.5 s two-way travel time (TWT) and 8 s TWT. The Moho reflector appears between 9 and 10 s TWT. Above the Moho, a clear reflector between the detachment and Moho is also imaged. It is interpreted as the top of an underplating body by comparison with wide-angle refraction

There is also no obvious crustal deformation across the Luzon-Ryukyu transform plate boundary. Furthermore, the sills were found at the northern end of the profile, southwestern offshore Taiwan. The black arrows mean “onlap” feature. Blue line unconformity T2, which occurred at 22 Ma. PC Penghu Canyon, DF deformation front. The rest of legends are the same as Fig. 2

study (Wang et al. 2006). Between CMP number 9000 and 12500, an un-deformed interface of basement is at 5.8 s TWT, but its seismic signature seems chaotic. Because a seamount is located nearby (Fig. 1), the nature of the basement could belong to mixed volcanic stratigraphic layers. In the north of the Formosa Canyon (Fig. 1), the seismic basement was also stretched considerably. An old symmetrical rifted graben at ca. 6 s TWT was located between CMP number 12500 and 19800. Another rifted graben feature was also found between CMP 22500 and 38000 (line MGL0905-20 in Fig. 6), east of section MGL0905-05. Based on high free-air gravity anomaly, relative low magnetization and the existence of symmetrical normal fault blocks (7–9 km in averaged crustal thickness in Fig. 9), this graben could consist of failed-rifted continental crust instead of oceanic crust. Under the

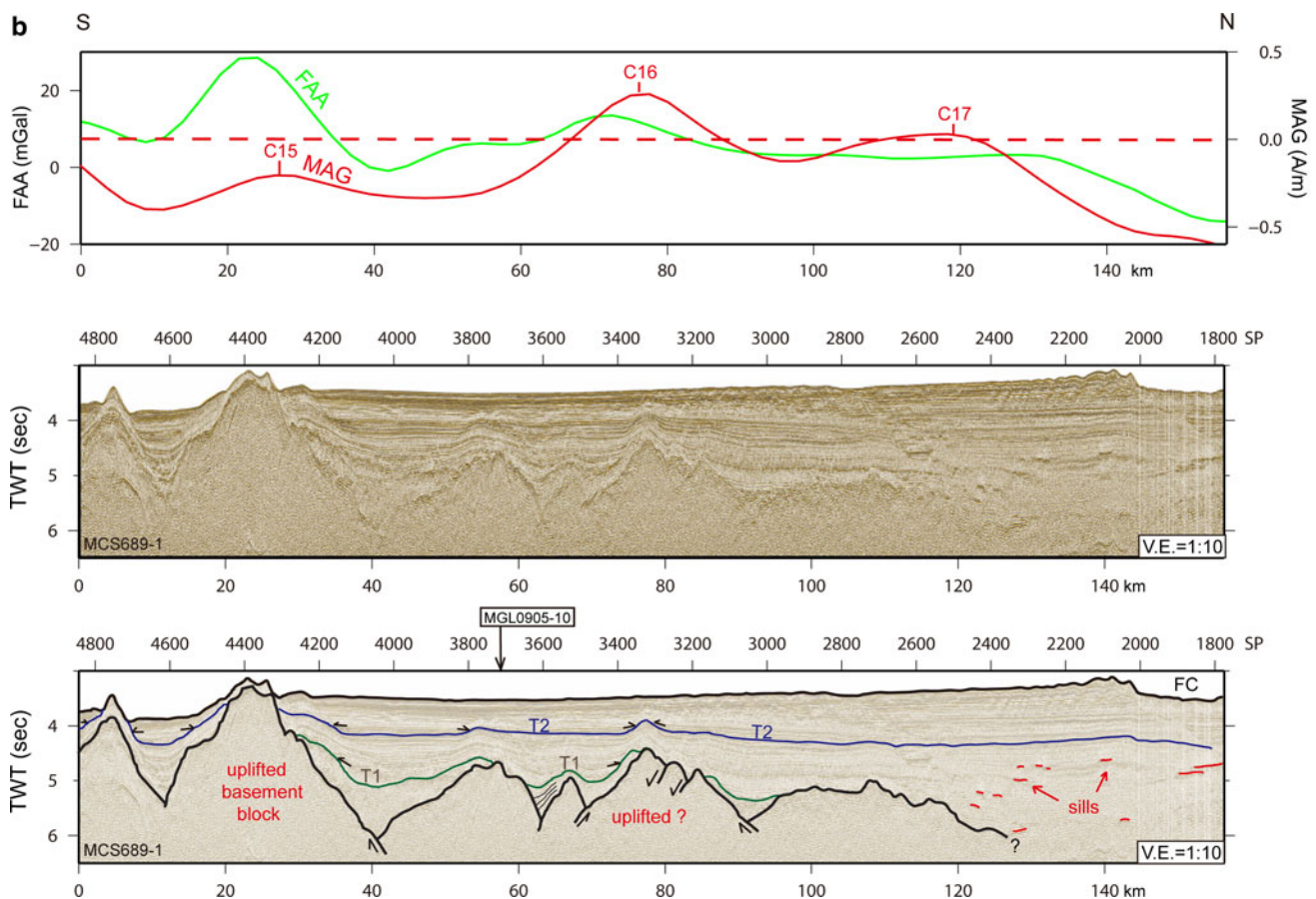


Fig. 3 continued

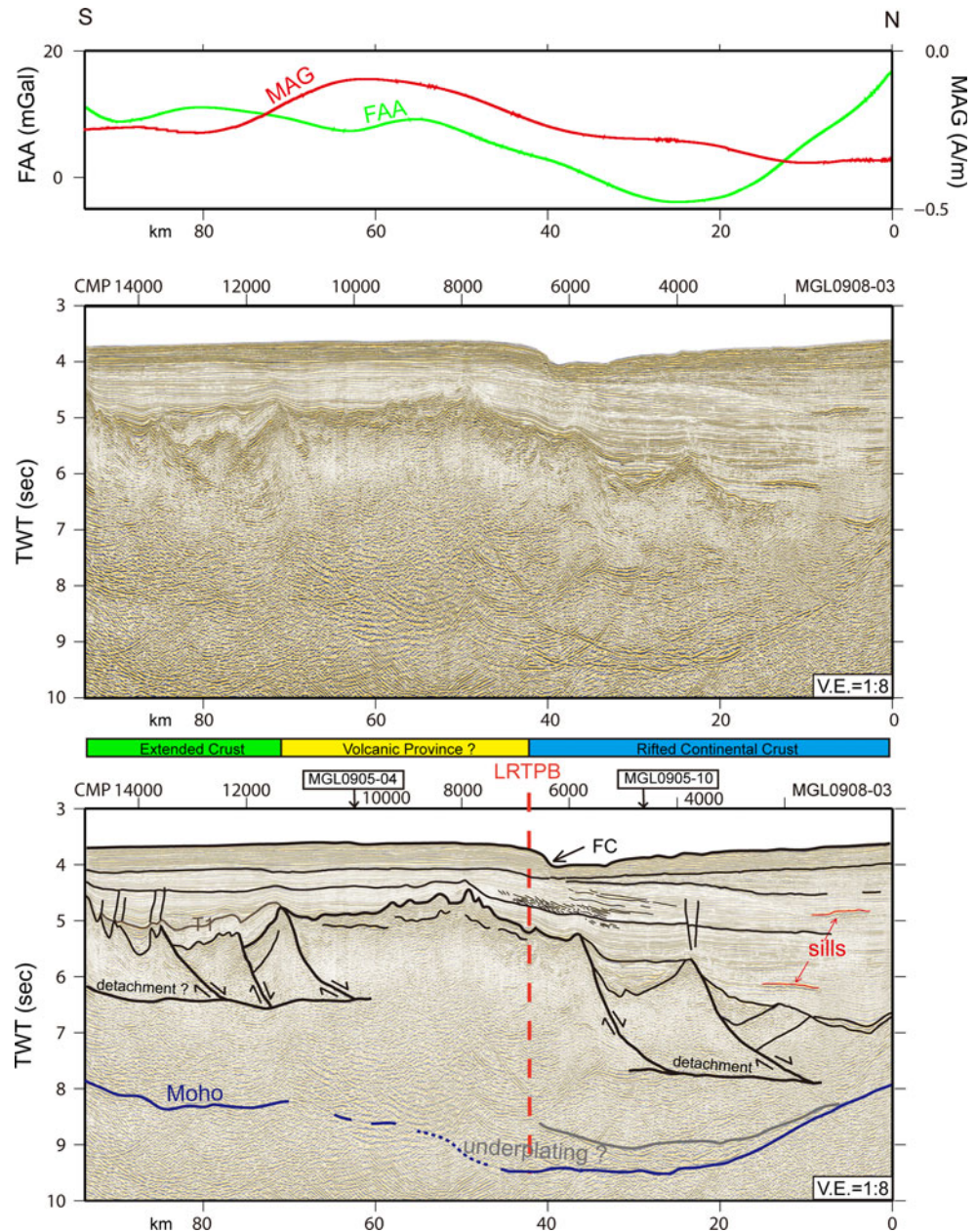
basement, an underplated body is also suggested beneath the graben. Between CMP number 24000 and 28272, listric normal faults dip northward from the basement to middle crust. Some normal faults even penetrate up to the seafloor as active faults. This extension is related to the rifting of the Tainan basin (Fig. 1) (Tseng 1994). In summary, two different kinds of tilted blocks were imaged along the profile: wide faulted blocks dipping landward with gliding syn-rift sediments, and a stretched horst and graben system with thin syn-rift sediments (~ 0.8 s TWT). These two stretched extensional systems are separated by the Luzon-Ryukyu transform plate boundary and could be formed by two different mechanisms.

LINES MGL0905-10 and MCS689-1 (Fig. 3a, b)

The line MGL0905-10 is located from the base of the SCS continental slope in the southwest to the Henchun accretionary prism (Fig. 1) in the northeast, off southwestern Taiwan. The average crustal thickness is about 4 s TWT (ca. 15 km, Fig. 9) in the south of the plate boundary and becomes thinner (ca. 8 km) in the north of it. Between CMP number 25000 and 50000, the basement was

extended and faulted into blocks dipping northeastward. The normal fault planes can also connect to a detachment beneath as line MGL0905-05 (Fig. 2). Above basement, a strong layering reflection (i.e. green layer) bounded a sequence which follows the basement relief generally between CMP 20000 and CMP 37500. This reflection is also found in the previous study, and corresponds to unconformity T1 (Yeh et al. 2010). As shown in Fig. 3a, the T1 unconformity is also attributed to be syn-rift in this profile. In the southwestern part of the profile, a significant uplifting of the basement was identified around CMP 46000. Another new unconformity T3 was also identified. If this ridge is old, the overriding sediments should present differential compaction. However, the T3 unconformity can connect to the seafloor then replaced by several possible landslide deposits between CMP 44500 and CMP 45500. This means the basement underwent an uplift event supposed to be close to the present day. An adjacent Dongsha volcanic uplift event occurred around 5.2 Ma (Lüdmann and Wong 1999) which caused a series of Miocene continental basement blocks to be uplifted reversely. The basement ridge at CMP 46000 corresponds to one of the uplifted blocks identified by Lüdmann and

Fig. 4 PSTM section of line MGL0908-03 and its seismic interpretations. As in previous seismic sections, the typical tilted fault blocks are heading toward the north between CMP 7000 and 16000. Further north, crust becomes extremely thin. The Moho is uplifted, which corresponds to raised gravity anomaly. This might be a local rifted basin. Note that the chaotic and strong reflection basement is imaged between CMP 7000 and 11500. It is difficult to trace the Moho reflection beneath basement and strong echoes are within the lower crust. This part of the crustal section belongs to volcanic intrusion. Sills are also found in this profile. In addition, the relative lower magnetization (<0 A/m) could also fit the interpretation of a rifting environment (oceanic fracture zones or continental rifting basin). The underplating layer could also be identified and is thinner than further south as MGL0905-10, which is about 0.5 s TWT. Further north, the underplating layer is diminished (CMP 1000). The legend is as in Fig. 2

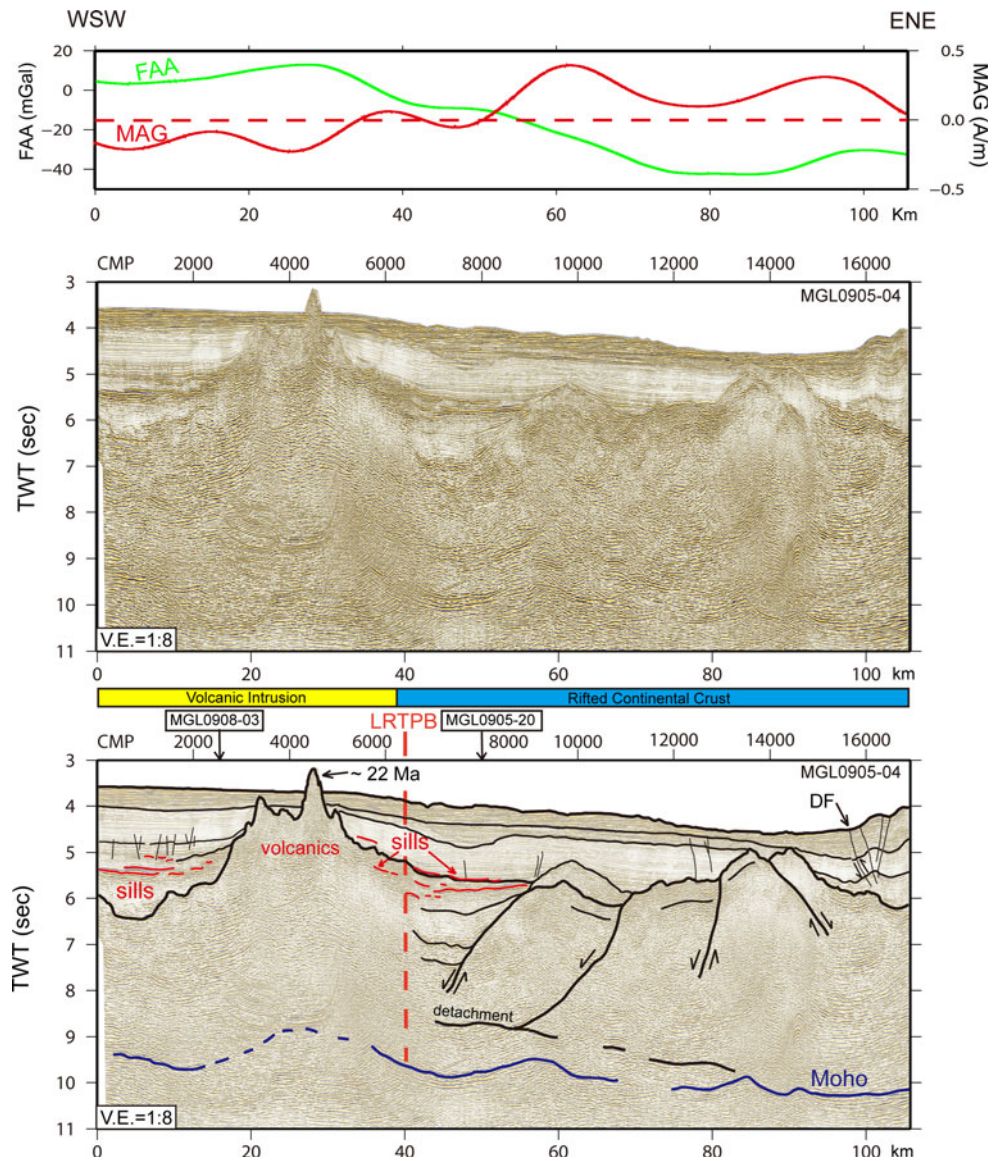


Wong (1999) as well as magnetic isochron C15 (Fig. 3a). Thus, this also implied that the uplifted fault blocks with intrusive volcanism could correlate to the occurrence of magnetic lineation.

The detachment reflection was also identified in this profile, as in the profile MGL0905-05. This strong reflector could be traced along the whole profile and is situated at the base of tilted crustal blocks. Furthermore, the underplating material is imaged and the layer is thicker (1 s TWT; 6.5 km) in the south and vanished northeastward (Fig. 10). Some reverse faults are observed near the tilted sediments around CMP 42500. Based on the seismic structures, tilted crustal blocks, existence of underplating layer and related intrusive events, the crust could belong to

thinned continental crust with volcanic intrusion rather than typical oceanic crust. However, the line MGL0905-10 is oblique to the orientation of magnetic lineations C15–C17 (Fig. 11). An old MCS profile (MCS689-1, Fig. 3b) was adapted to discussion (Yeh and Hsu 2004). As MGL0905-10 shows, several uplifted basement blocks were found at SP 4800, SP 4400, and a minor one at SP 3300. Except for the isochron C17, the magnetic reversals seem to be more and less consistent with the basement relief. However, the basement block at SP 3300 (corresponds to CMP 34000, line MGL0905-10) has 0.25 A/m magnetization that is higher than the basement uplift area in the south. Thus, the magnetization variation is not dominated by basement relief. We cannot neglect the

Fig. 5 PSTM section of line MGL0905-04 and its seismic interpretations. The obvious volcanic extrusion is identified between CMP 7000 and 2000. Note that the abundant sills surround and flowed out from the extrusive seamount. Between CMP 7000 and 11000, clear crustal faults dip SW, which marks the extension phase. Another normal fault dipped trenchward that could be related to the subduction. The magnetization is high between CMP 9000 and 16922 that refers to volcanic crustal characteristics. The legend is as in Fig. 2



possibility that the crustal characteristics could be volcanic in origin.

LINE MGL0908-03 (Fig. 4)

This profile is north–south trending and is perpendicular to the general spreading direction of the SCS. The averaged crustal thickness is about 3.5 s TWT (13 km) in the south of plate boundary, which is slightly thinner than in previous profiles. As mentioned previously, the brittle and faulted basement is also imaged in the upper portion of the crust. The main tilted blocks along the profile are between CMP 11000 and CMP 16000 and between CMP 2000 and CMP 6000. The faulted blocks dip northward at depth of ca. 5.5 s TWT and their bases connect to a detachment near 7–8 s TWT. As mentioned previously, the overlapping sedimentary sequence is clearly sub-parallel to the top of the

basement block, which could belong to syn-rifting sedimentary column that separated upper sediments from unconformity T1. From CMP 6000 and CMP 11000, the thin sediments overlapped on a chaotic basement. The interface between sedimentary column and basement is blurred. In addition, the Moho reflection beneath this part of the basement is missing. This probably also implies the existence of a high-velocity layer beneath. The magnetization of this part of the section is relative high, which may also imply volcanic intrusion. However, magnetization value is negative along the whole profile, and that shows character of oceanic fracture zone or rifting basin basement fractured area. In the north, the crust is almost broken up in the northern end of the profile. The crustal thickness is less than 1 s TWT (about 8 km) accompanied by very thin syn-rifting sediments (~0.5 s TWT) and no disturbance of overlapping sediments. Based on high free-air gravity anomaly (Fig. 1),

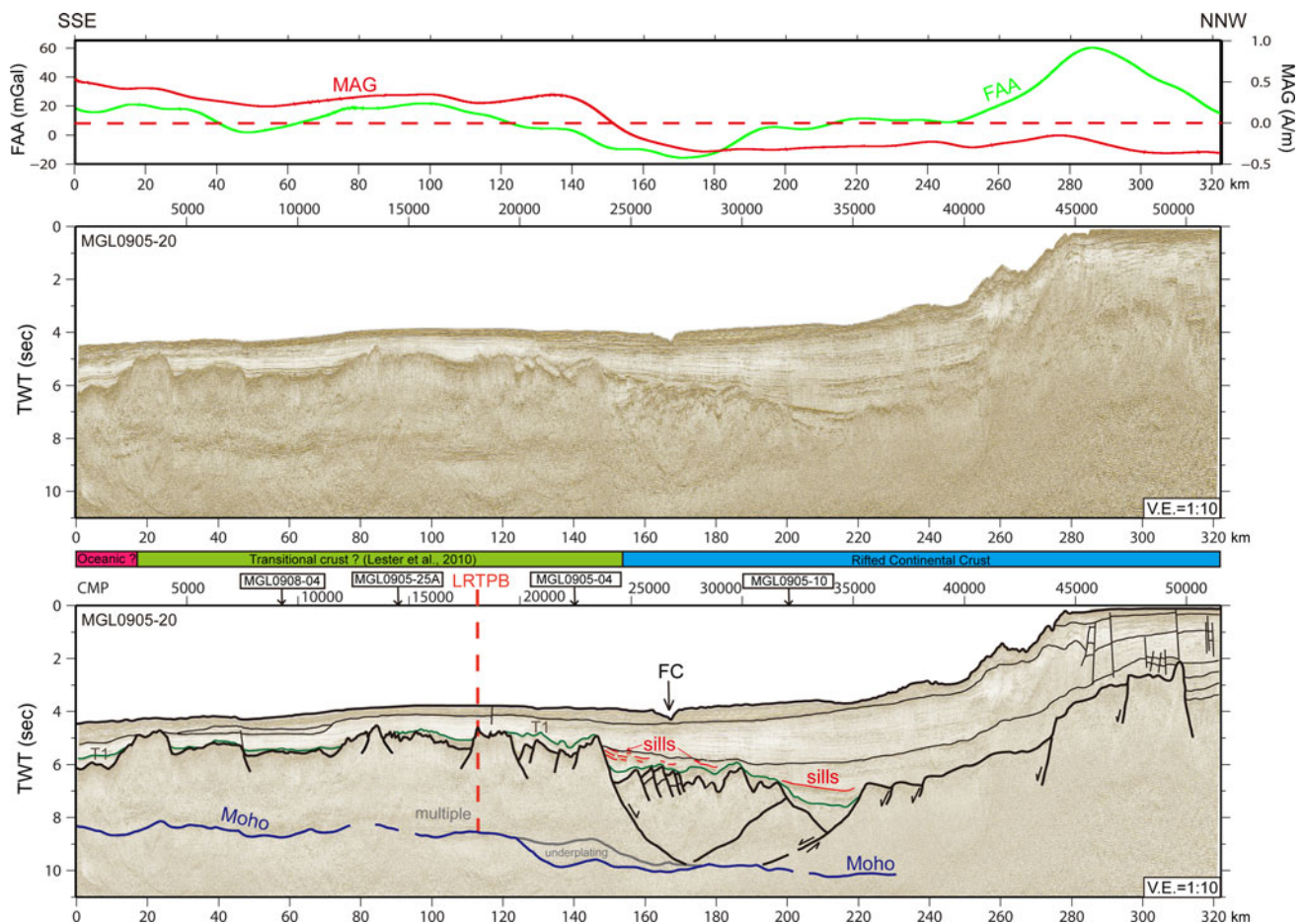


Fig. 6 PSTM section of line MGL0905-20 and its seismic interpretations. This profile is a typical example from pure oceanic crust to rifted continent. Note that between CMP 0 and 23000, the basement relief is smooth and has chaotic crustal reflection. The crustal thickness is between 2 and 4 s TWT, which is about 12–14 km. The crust is still thick compared to typical oceanic crust. The magnetization is positive in this region. A recent OBS refraction study constrains the crust between CMP 2500 and 25000 as belonging to

continent–ocean transition (Lester et al. 2010). The positive magnetization corresponds to volcanic intrusions. North of CMP 23000, obvious crustal extension blocks occur and form a local rift basin. In addition, between CMP 40000 and 51455, the basement rises to 3 s TWT corresponding to higher gravity anomaly. However, the corresponding magnetization is negative, meaning that the crustal characteristic is non-volcanic. The legend is as in Fig. 2

relative low magnetization (Fig. 11) and existence of symmetrical normal fault blocks (Figs. 4, 6), this graben could refer to fail rifted continental crust instead of oceanic crust. The beta factor is equal to 3.125 ($\beta = 25/8 = 3.125$; 8 km: final crustal thickness; 25 km: initial crustal thickness).

LINE MGL0905-04 (Fig. 5)

As a typical volcanic intrusive or extrusive body, the acoustic basement shows chaotic reflections between CMP 0 and CMP 6500. Several high-amplitude reflection layers (i.e. bright spot) parallel to adjacent sedimentary sequence could be traced back to an extrusive volcano. Considering a local source of magma supply, we speculate the high-amplitude reflection layers are intrusive sills (Fig. 5). An Ar–Ar dating and geochemical analysis of dredged rocks

on top of the extrusive submarine volcano shows existence of EM (enriched mantle) type II plume type basalts in 22 Ma (Chung et al. 1995; Hsu et al. 2004). In addition, the magnetization of erupted volcano is reversal to normal magnetized rocks. We can attribute this volcanism to its occurrence in a magnetic reversal epoch with respect to the present-day geomagnetic field. Between CMP 6500 and CMP 9000, a basement low filled with 4 s TWT thick sediment was associated with a former extensional deformation. Due to the only differential compaction effect in the whole overlapping sequence, this extensional event probably is onset of basement rifting (syn-rift). In addition, in the area between CMP 9000 and CMP 16922, magnetization value is relatively high and positive varies from 0 to 0.4 A/m. The crust here probably belongs to transition between continental and oceanic crust with volcanism.

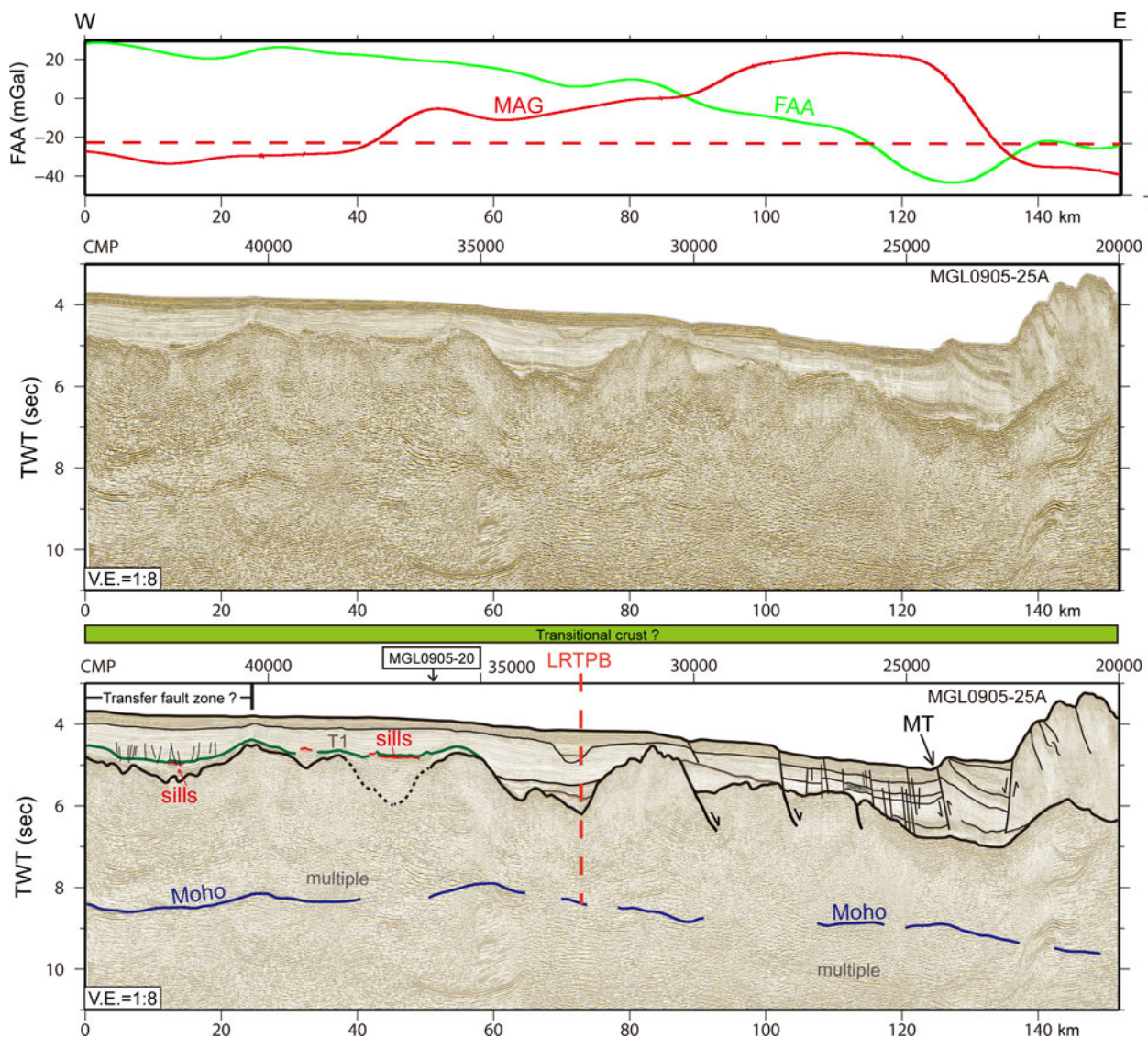


Fig. 7 PSTM section of line MGL0905-25A and its seismic interpretations. Note that the basement relief is smoother than in previous profiles. The crustal thickness is about 3 s TWT, that is also thinner

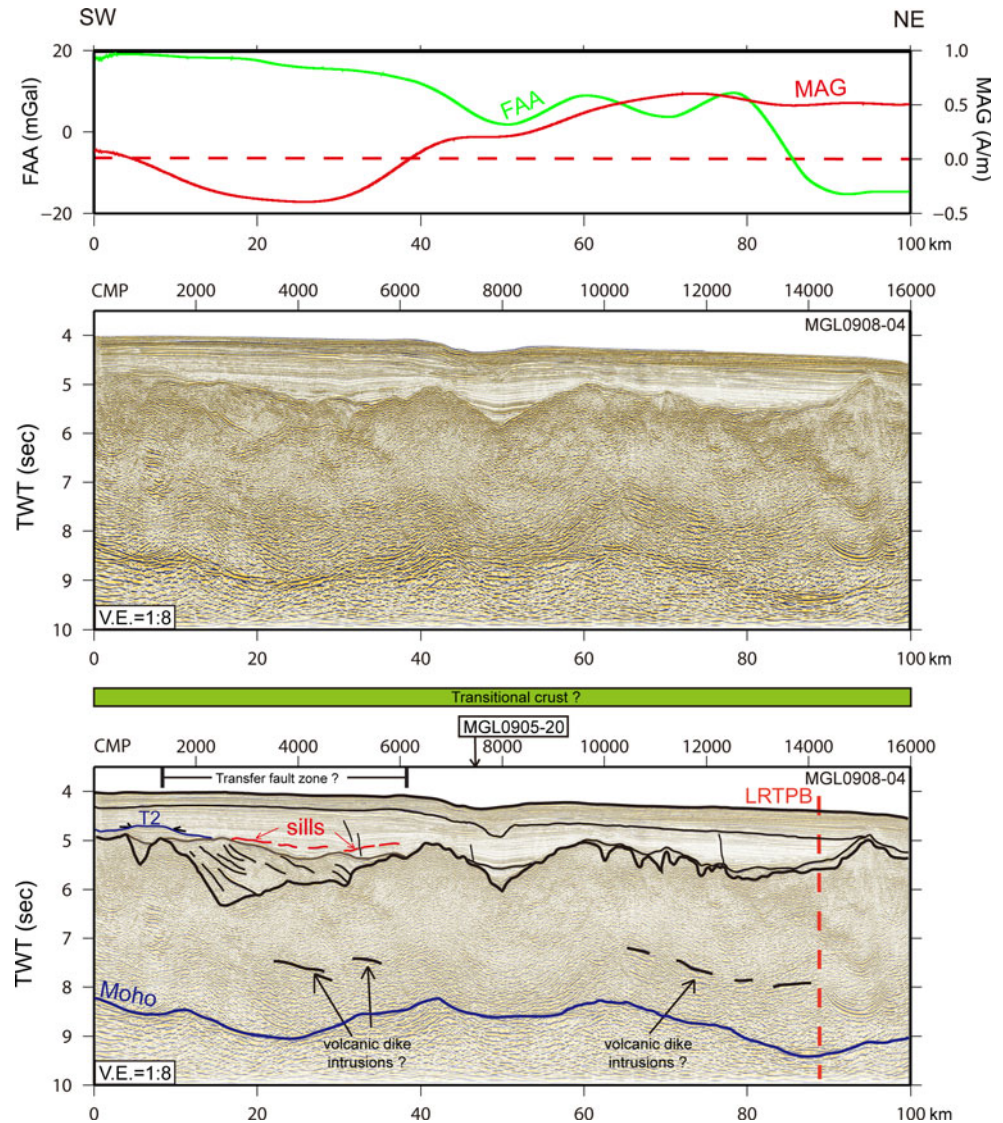
than MGL0905-10. The magnetization is relatively high (0–1 A/m), indicating a volcanic origin. The legend is as in Fig. 2

LINE MGL0905-20 (Fig. 6)

The magnetization profile in Fig. 6 illustrates a good example from oceanic crust (i.e. isochron C12; Fig. 11) to rifted continental crust. Overall, the basement has chaotic reflection between CMP 0 and CMP 10000 and crustal thickness is 2 s TWT on average (about 12 km), which is compatible with the result of a recent OBS refraction study (Lester et al. 2010). Lester et al. (2010) suggested that the crust between CMP 0 and CMP 22500 is transitional crust. However, the magnetization is positive. White et al. (2008) suggested the upper crust and lower crust of the transitional crust was intruded by basaltic magma as inner crustal reflection in the Hatton bank margin. The inner crustal reflection is also imaged. This may explain why the thick

crust (i.e. 12 km in averaged) has positive magnetization. However, although the lower crustal material was imaged in this area (Figs. 2, 3, 4, 5, 6), the basalt eruptions associated with seaward-dipping reflectors are not found. Further north (CMP 22000 and CMP 23000); the basement was fractured highly with listric normal faults accompanied by typical collapsed graben, just beneath Formosa Canyon. The crust was thinned from 12 km in the south to less than 8 km in the north (Fig. 9). To CMP 34000, the basement was highly stretched with thinnest crust (~ 5 km). In addition, the magnetization is relatively low (-0.4 A/m) that could be associated with fractured crust. Thus, this graben between Formosa canyon and the northern South China Sea continental slope could imply a rifted continental origin. Between CMP 35000 and 55000, the seafloor

Fig. 8 PSTM section of line MGL0908-04 and its seismic interpretations. As in line MGL0905-25A, the crustal thickness is 3 s TWT and has smooth basement relief. Note that there are some inner crustal reflections which may correspond to magma injection based on a previous study (White et al. 2008). The magnetization is also high (0–0.5 A/m) except for the section between CMP 1800 and 7000. The legend is as in Fig. 2



becomes rugged and steep, that is the area from continental slope to continental shelf. In this area, where the thickest sediments were deposited, the irregular, discontinuous seismic reflection marks its inferred turbidite deposits character. Up to the shelf, some normal faults have penetrated to the seafloor as active faults which are associated with tectonic activity of the Tainan basin (Tseng 1994; Lin et al. 2003).

LINE MGL0905-25A (Fig. 7)

The E-W trending profile is across the main northern South China Sea basin and cuts cross the Manila Trench, which exhibits typical subduction characteristics (i.e. bending-related normal faults and thrusts in the sedimentary column). Between CMP 44823 and CMP 32000, the shallow sedimentary column (about 1 s TWT below seafloor) is flat

and shows no deformation. This implies that no active tectonic event corresponds to basement in this area currently. From CMP 31000 to CMP 20000, the crust starts to bend with normal faults and has subducted eastward. The deformation style changes from extension to thrust near CMP 24000. For the crustal part, the seismic reflection is different from the profile MGL0905-10 (Fig. 3a) which shows chaotic and rare inner crustal reflection. This indicated that the crustal nature tended toward volcanic. However, the crustal thickness is from 8 to 10 km in general (Fig. 9) which is still thicker than typical oceanic crust. Magnetization varies from -0.1 to 1 A/m which may be attributed either to oceanic crust or transitional crust. However, an OBS refraction study (Lester et al. 2010) suggested a transitional crustal nature at CMP 37000. Thus, this positive magnetization (0–0.5 A/m) might refer to intrusive volcanism as evidence of sills.

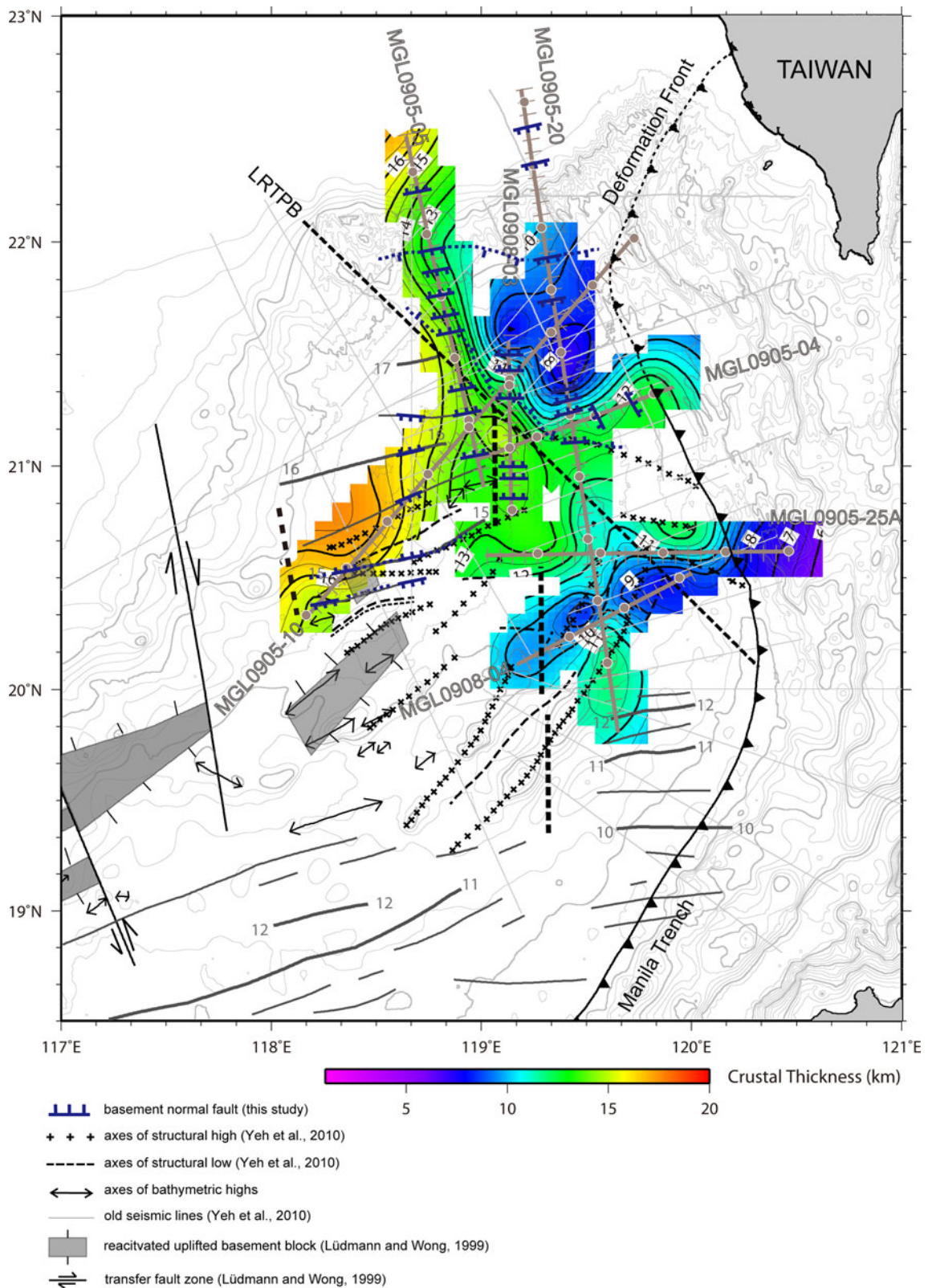


Fig. 9 Crustal thickness in kilometers. The average crustal thickness beneath the South China Sea varies from 6.5 km (southeastern area) to 17 km (close to its northwestern margin). Note that a thin crust area (~5 km) is located at 21°30'N, 119°10'E that indicates a local rifted

graben. There is no obvious crustal thickness difference along and across the Luzon-Ryukyu transform plate boundary. The other symbols are as in Fig. 1

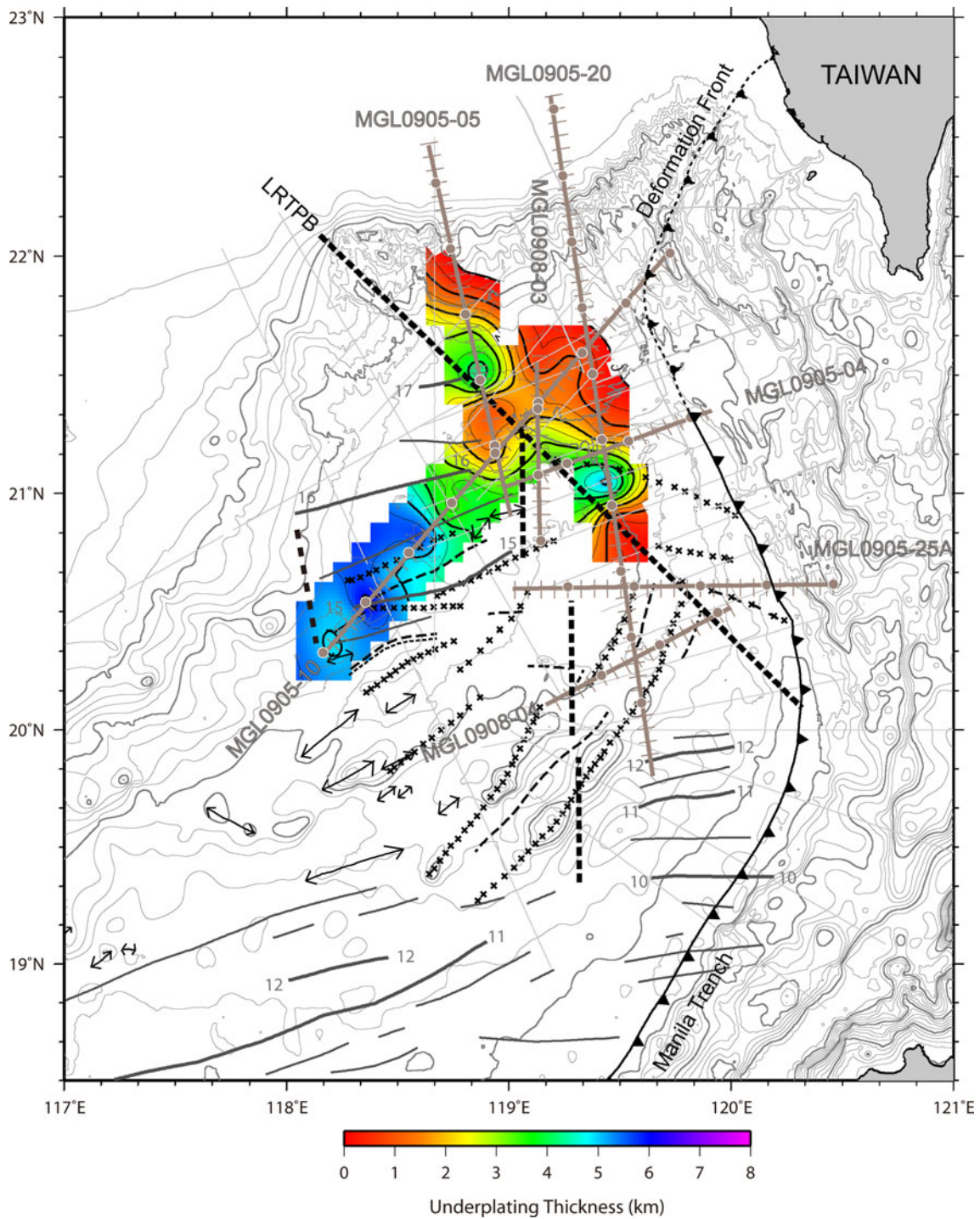


Fig. 10 Thickness of lower crustal material in kilometers. The thickness is greatest at 6.5 km in the south and diminishes south of the northernmost South China Sea margin. Note that the *thickest one* is

located at the base of NE-SW trending South China Sea margin. The other *symbols* are as in Fig. 1

LINE MGL0908-04 (Fig. 8)

Like line MGL0905-25A, the Moho appears around 8–9 s TWT. The acoustic basement shows irregular and chaotic reflection that fits the character of volcanic crust. Between

CMP 0 and CMP 6200, a tilted sedimentary sequence was truncated by unconformity T1, above which almost flat sediments are shown in the southern end of line MGL0905-20. This indicates that the extension event is syn-rift, not post-rift. This extensional event may occur along crust

fractured area that is compatible with relatively low magnetization. South of CMP 2000, a sedimentary sequence overlapped the syn-rift unconformity T1 formed as a bulge like unconformity T2 that is associated with volcanic uplift (Lüdmann and Wong 1999; Yeh et al. 2010). After CMP 6500 to the northeast end, the magnetization appears positive and high (~ 0.5 A/m) generally with relative thinner crust (< 9 km), indicating the crustal characteristics is still transitional crust. In the left end of profile, the magnetization value is negative, which could be related to a transfer fault zone or extended crust bounding the magnetic isochrons C15–C17 in the east (Fig. 11).

Discussions

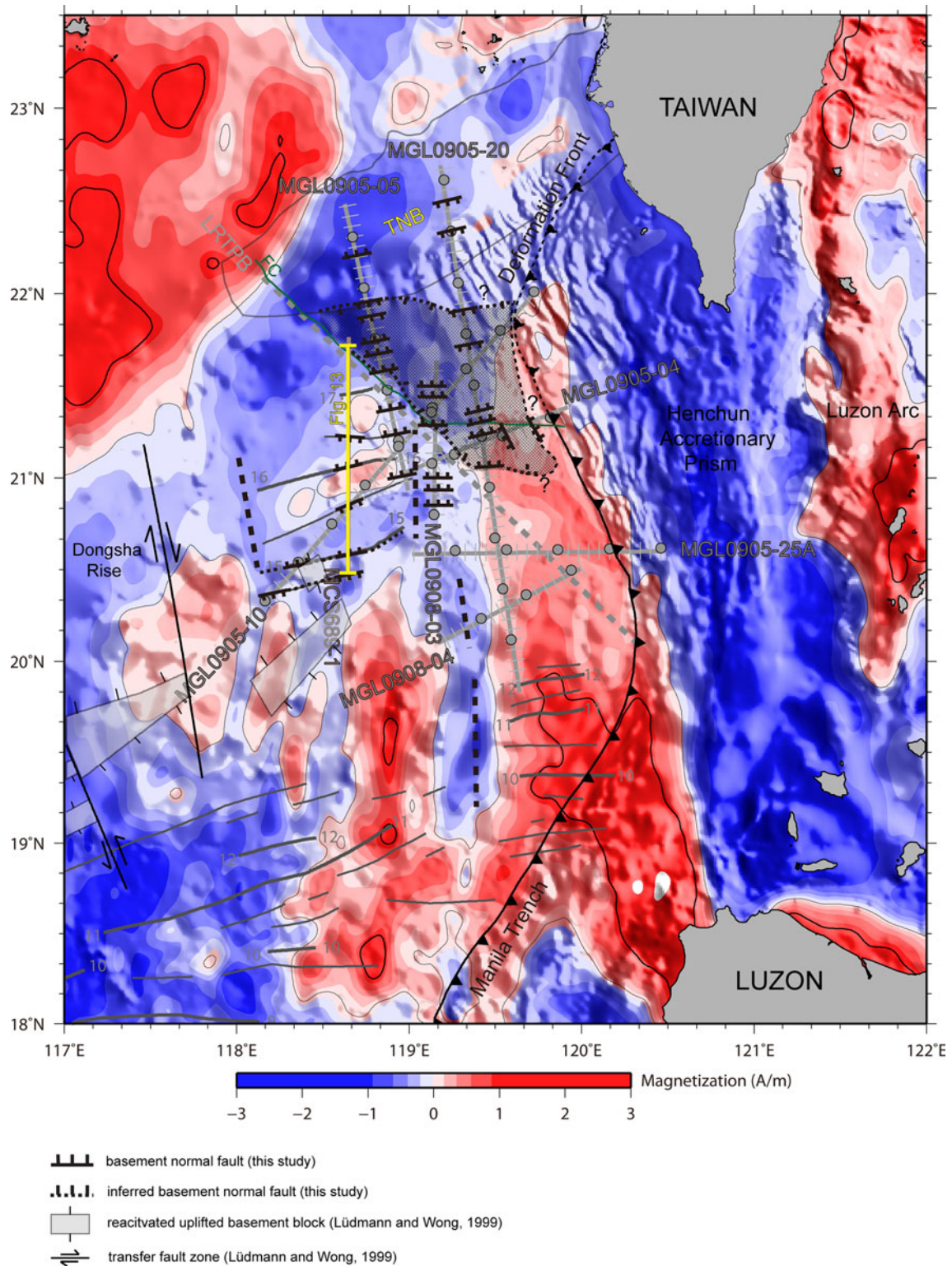
As shown in Fig. 3a, b, two profiles cut across the pre-identified oceanic terrane (i.e. isochron C15–C17) (Hsu et al. 2004; Yeh and Hsu 2004; Yeh et al. 2010). However, obvious basement listric faults are present in the upper crust. A significant existence of a lower crustal magmatic body is imaged underneath the lower crust. As the indicator, lower crustal material (LCM) often appears at the continent–ocean transition area that is related to lower crustal partial melting induced by decompression mantle convection during the continental rifting period. In this study, the LCM is thicker (~ 6.5 km) southward along the line MGL0905-10 (Figs. 3a, 10), then is gradually thinner northward and pinch out southwest of deformation front (Figs. 3a, 10). Compared to the interval velocity determined by pre-stack time migration of line MGL0905-10 (Fig. 12) and previous refraction velocity from OBS2006 (Wang et al. 2006), velocity of this lower crustal body is between 7.2 and 7.5 km/s. This velocity is higher than either normal lower continental crust or oceanic crust layer II at 6.8–7.0 km/s, which also could be interpreted as LCM. This LCM could also be found at other magma-rich margins such as Newfoundland, Greenland, and Vøring (Mjelde et al. 2002; Voss and Jokat 2007). In addition, the PSTM velocity reveals perfect fit to an average velocity variation in the Hatton Bank (White et al. 2008) in the upper crust (< 10 km). This implied that the upper crust of isochron C15–C17 area included basaltic intrusions similar to Hatton Bank margin. However, the velocity of the lower part of the crust (10–20 km) in this study is higher than Hatton Bank. This indicates that the upper-crustal magmatic intrusions and LCM co-exist in the magnetic area C15–C17.

Figure 9 shows the crustal thickness of the study area. The thinnest crustal thickness is about 5 km north of the Luzon-Ryukyu transform plate boundary associated with negative magnetization and higher Bouguer gravity anomaly (Yeh and Hsu 2004) and symmetrical normal

faulted blocks in the upper crust. Therefore, it is reasonable to interpret it as a rifted continental graben. Another thinner crust area is located at $20^{\circ}20'N$, $119^{\circ}20'E$, that varies from 8 to 10 km that is associated with higher magnetization (0.5–1 A/m) and rare crustal faults. However, the inner crustal seismic reflection as the top of LCM is still existed. The crustal characteristics should be referred to continent and ocean transition. Figure 10 shows the spatial distribution of LCM thickness in kilometers. The maximum thickness of the LCM is about 6.5 km, located at the bottom of NE-SW trending northern SCS margin at $118^{\circ}20'E$ and $20^{\circ}30'N$. The LCM of this area might be related to the continental rifting process at the NE–SW trending margin. Lüdmann and Wong (1999) identified several rifted continental fault blocks that were reactivated then uplifted twice by volcanic uplift: Miocene uplift and the Dongsha uplift event (i.e. 5.2 Ma), respectively. The magma supply of syn-rift to post-rift uplifted events resulted in LCM. This interpretation is also compatible with the results of previous two ship-based expanding spread profile (ESP) experiments (ESP eastern transect) with a > 7.0 km/s magmatic body attached to the lower crust (Nissen et al. 1995). Moreover, another post-rifting volcanism occurred at 22 Ma which affected areas from the northern South China Sea to western Taiwan (Yen 1958; Chung et al. 1995). The sills and intrusive/extrusive volcanic bodies were identified in most of the MCS profiles, which is compatible with previous studies (Lin et al. 2003, 2009; Sibuet et al. 2002). In summary, plenty of magmatic events were imprinted to the northern SCS area from late Oligocene to Pliocene time. Based on the definition of characteristics of passive margin, the northern SCS margin could be classified as a volcanic margin.

To constrain the crustal characteristics of isochron C15–C17 area, we performed forward magnetic modeling. Two kinds of crustal models were examined: rifted continental crust with volcanism and thick oceanic crust. Although the line MGL0905-10 can image whole crustal section, it is oblique to the C15–C17 magnetic reversal. Considering the crustal structure is more or less coherent in the adjacent area, we adopted the seismic interpretation of line MCS689-1 perpendicular to C15–C17 lineation for building the synthetic models. The Moho depth was set to be constant as 17 km in depth. The declination and inclination were set the same as present day, at -2.93° and 31.92° . The synthetic results are shown in Fig. 13a.

As Fig. 13b shows, we assumed the bedrock is dominated by extended continental crust with several intrusive volcanic bodies. The thickness of LCM was also adopted by interpretation of line MGL0905-10. The intrusive volcanic bodies were assumed to be basaltic with 2 A/m magnetization on average. As Fig. 13a shows, the synthetic magnetic anomaly is fit well to the observation between 0



and 40 km in distance. In contrast, the synthetic anomaly is an obvious underestimate from 70 km to the northern end of the profile. To fit the biggest magnetic anomaly at 60 km in distance, magnetization 7 A/m had to be used. This magnetic susceptibility is ambiguous for typical intrusive

or extrusive volcanic bodies. In addition, the result also implied the large magnetic anomaly variation may generate from bigger magnetic susceptibility contrast of the crustal volume between 80 and 160 km. The Luzon-Ryukyu transform plate boundary separates fluctuated magnetic

Fig. 11 The inverted magnetization draped on bathymetry. The *thin black polygons* indicate a region which is larger than 0 A/m; *bold polygons* show a region which is larger than 1 A/m. Note that the similar magnetization value (close to 1 A/m) both north and south of the Luzon-Ryukyu transform plate boundary east of 119°E. The MCS lines (MGL0905-05, MGL0905-10, MGL0905-04 and MGL0908-03) are close to or across the low magnetization area. In addition, striped magnetization (i.e. close to 0 A/m) is located south of the Luzon-Ryukyu boundary that presents magnetic reversal and -1.5 to 0 A/m north of the Luzon-Ryukyu boundary, west of 119°E. The relative low magnetization zones in between magnetic striped patterns may refer to transfer fault. The extreme low value (-1 to ~ -3 A/m) zone is along the northern South China Sea shelf break which corresponds to sedimentary basin or crustal fractured area. It is noted that a series of uplifted basement blocks corresponds to magnetic stripes C15–C17. In the end of profiles MCS689-1 and MGL0905-10, an obvious uplifted basement block is also reported by Lüdmann and Wong (1999). These blocks were identified as reactivated rifted continental blocks (Lüdmann and Wong 1999). *Meshed area* symmetrical rifted graben north of the Luzon-Ryukyu transform plate boundary; *Light grey* MCS track lines used in this study. *Dashed black lines* transfer fault zones identified by magnetization. *Dark grey lines* magnetic lineation identified by Yeh et al. (2010). The bathymetric contour interval is 200 meters. The *bold N–S yellow line* shows a forward magnetic model that is presented in Fig. 13

anomaly in the south from magnetic quiet area north of it. Figure 13c is a thick oceanic crust model adopted by a magnetic age identification study (Hsu et al. 2004). The susceptibility model was supposed to be striped way (i.e. \pm magnetization value). The result shows that the synthetic magnetic anomaly could fit the observation better than thinned continental model. However, there are still discrepancies at 50 km (i.e. small magnetic reversal event) and north of 80 km in distance. In fact, only a crustal column at 60 km (isochron C16) conserved positive magnetization (0.25 A/m, Fig. 3b), which is less than typical oceanic crust (i.e. 2 A/m). The other two magnetic reversals (C15 and C17) are negative magnetization. Hsu et al. (2004) suggested the C15–C17 underwent post-spreading volcanism then caused reduced magnetization. However, except for syn-rift Oligocene lower crustal underplating, all other magmatic events are post-rift (i.e. 22 and 5.2 Ma). The rotated listric basement fault blocks connected to a detachment in the upper crust indicates a ductile layer (i.e. lower crust or mantle) was needed to introduce for driving the brittle fault blocks mechanically. Although the detachment fault was also found at oceanic crust, the extension was occurred at slow or very slow spreading ridge or transform fault area. If that is the case, the oceanic core complex (i.e. gabbro and mantle peridotite) should be discovered and the crustal thickness is less than 8 km (Dannowski et al. 2010) approximately in the Mid- Atlantic Ridge. In contrast, the crustal thickness varies from 12 km to 17 km in the study area, which is too thick for oceanic crust (Fig. 9). In addition, the observed velocity variation is not fit to thick oceanic crust (Fig. 12).

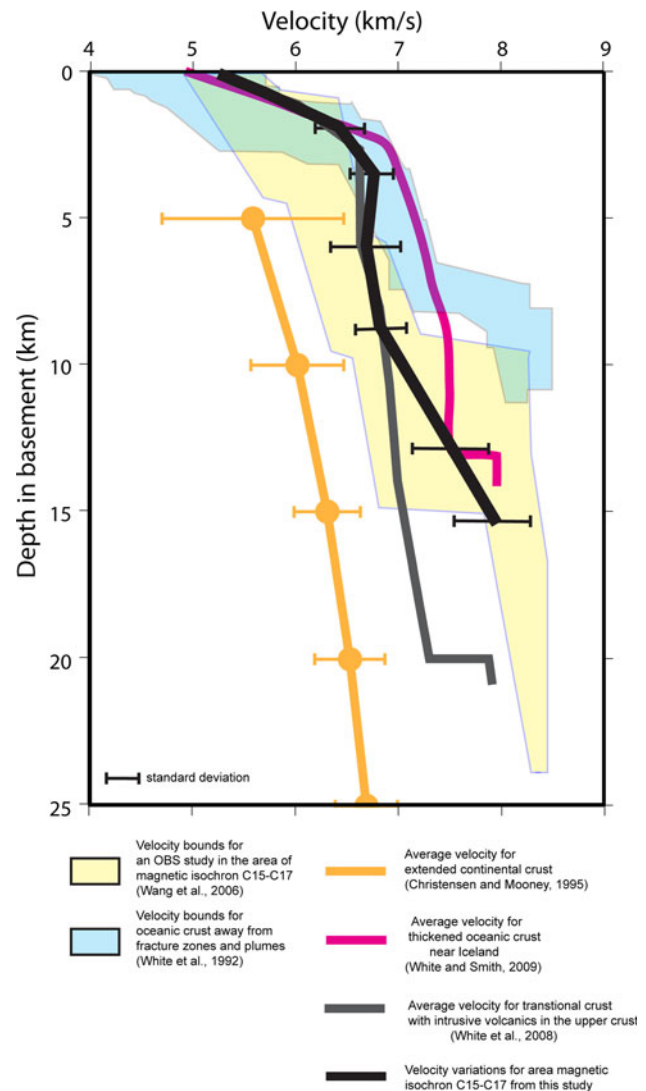


Fig. 12 Comparison of thick oceanic crust (White and Smith 2009), typical oceanic crust (White et al. 1992), rifted continental crust (Christensen and Mooney 1995), and transitional crust with basaltic intrusions in the upper crust (White et al. 2008) to interval velocity derived from pre-stack migration processing of line MGL0905-10 between CMP 28000 and 40000. The velocity was adopted every 200 CMP. Note that the velocity variation follows perfectly to the intrusive upper crust of transitional crust trend in the upper 10 km. The thickness of lower crustal material is about 7 km here on average

In summary, the crustal structure at magnetic area C15–C17 refers to magmatic intrusive upper crust and lower crustal material, based on crustal velocity variation. The crustal nature should belong to continent and ocean transition. However, forward magnetic modeling suggested the crust developed in striped way as oceanic crust. Therefore, the magnetic reversals could be created as two ways: basaltic magma injection along crustal weakness (Russell and Whitmarsh 2003) or a relict undiscovered ancient oceanic crust piece beneath. In addition, the misfit between

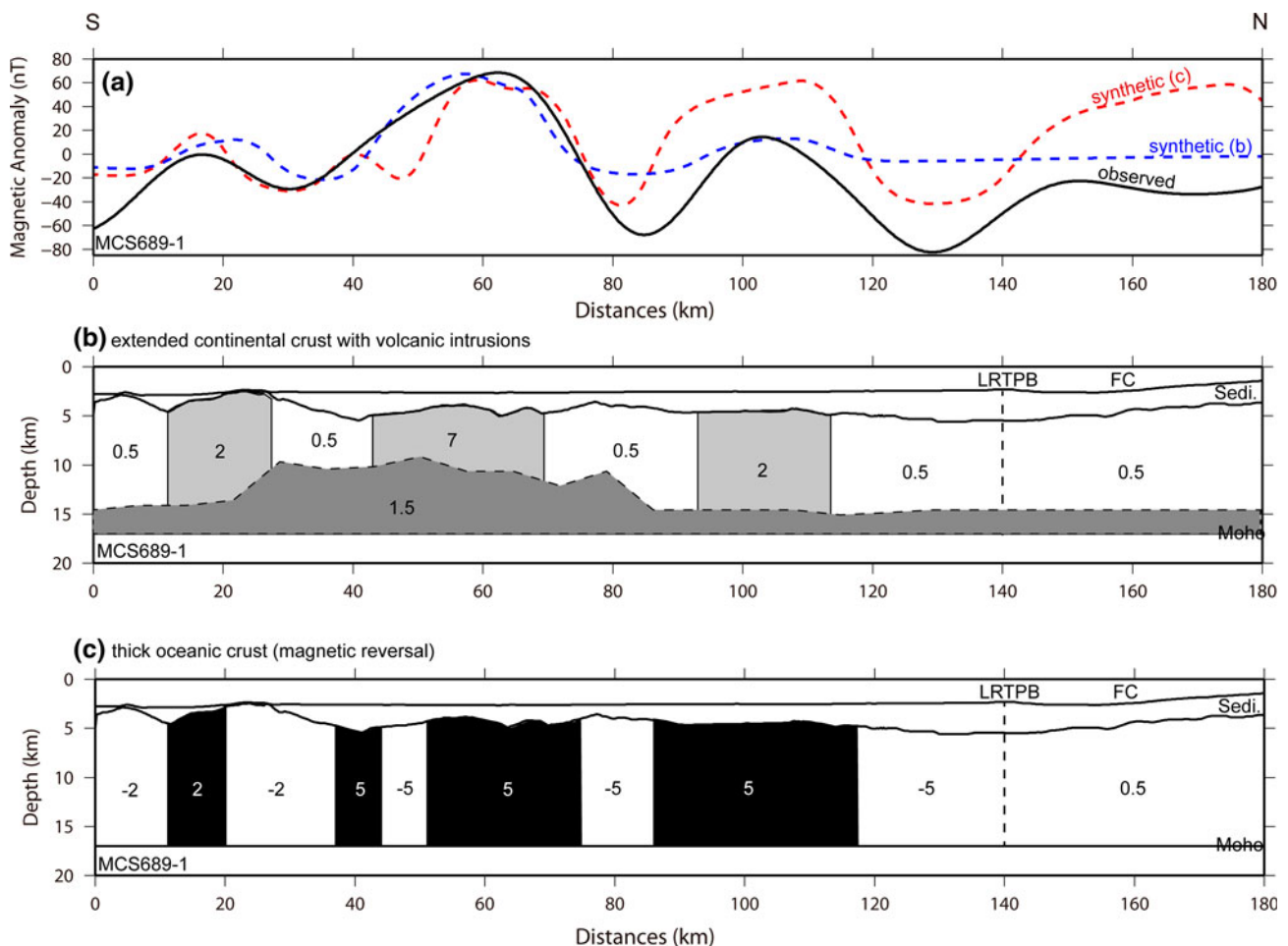


Fig. 13 Forward magnetic models. The basement relief was adopted by seismic interpretation of line MCS689-1 (Fig. 3b). The Moho discontinuity was set to 17 km based on the seismic interpretation of MGL0905-10 (Fig. 3a). **a** Observed magnetic anomaly and synthetic magnetic anomaly from two crustal models; **b** thinned continental model with intrusive volcanism; **c** thick oceanic crust model; noted

that the thick oceanic crust model has better fit to the observation. However, both models contain discrepancy between synthetic and observation especially north of 60 km in distance. The magnetic susceptibility unit is A/m; *Sedi.* sedimentary column, *FC* Formosa Canyon, *L RTPB* Luzon-Ryukyu transform plate boundary

synthetic magnetic anomaly and observation also indicated some crustal structure discrimination is still unknown.

Conclusions

The crust in the northernmost South China Sea has undergone several different magmatic events that cause its complicated crustal nature. The newly collected MCS data were processed by pre-stack time migration (PSTM) that provides image for the whole crustal picture in the study area. In general, the syn-rift extension is found to be clustered along the NE-SW trending South China Sea margin. Three kinds of rotated fault blocks are identified: (1) Wide basement tilted blocks in the upper crust south of the Luzon-Ryukyu transform plate boundary. The bottom of those fault planes can connect to a quasi-horizontal

detachment. Some tilted blocks were re-activated and uplifted, affected by Miocene volcanism and the Pliocene Dongsha uplift event. (2) A symmetrical rifted graben with the thinnest crust of 5 km is located between the Tainan basin and the Luzon-Ryukyu boundary. The negative magnetization may constrain its rifted continental origin. (3) Gravity gliding normal faults heading southward is in the northernmost South China Sea margin. Significant magmatic lower crustal material (LCM) is imaged in the study area. The thickest LCM is 6.5 km that has caused 17 km total crustal thickness in the magnetic isochron C15. The interval velocity variation derived from PSTM processing in the magnetic isochron C15–C17 area suggests that the crust is composed of magmatic intrusions in the upper crust and a separate intrusive body LCM in the lower crust. The crustal nature should be attributed to a transition zone between continental and oceanic crust. Nevertheless,

forward magnetic modeling suggests that the whole crustal thickness was magnetized in striped way as oceanic crust. However, the magnetic reversals of the crust may also be caused by either magmatic intrusion across a magnetic reversal epoch or relict undiscovered ancient oceanic crust. The crustal structure discrimination needs to be confirmed by future OBS and deep ocean drilling studies.

Acknowledgment We are grateful for scientific party of the Marine TAIGER during Legs MGL0905 and MGL0908. This study was done partly during Y.-C. Yeh's visit to the Department of Geology & Geophysics, University of Hawaii at Manoa. We thank Profs Kirk D. McIntosh, Francis Wu and Dr. Philippe Schnürle for fulfilling discussions and suggestions onboard R/V *Marcus G. Langseth*. Special thanks to Profs G. F. Moore, Brian Taylor and Miss Masako Robb for discussions on tectonics and seismic processing and interpretation techniques. The constructive comments from both two anonymous reviewers and Chief Editor Dr. Amy Draut help to revise this paper that is appreciated very much. This study was supported by National Science Council (NSC100-2116-M-019-006), Taiwan.

References

- Barckhausen U, Roeser HA (2004) Seafloor spreading anomalies in South China Sea revisited. In: Clift P, Wang P, Kuhnt W, Hayes D (eds) Continent-ocean interactions within east Asian marginal seas. Geophysical monograph, vol 149. American Geophysical Union, Washington, pp 121–125
- Berndt C, Skogly OP, Planke S, Eldholm O, Mjelde R (2000) High velocity break-up related sills in the Vøring Basin off Norway. *J Geophys Res* 105(28):443–428, 455
- Briaux A, Patriat P, Tapponnier P (1993) Updated interpretation of magnetic anomalies and seafloor spreading stages in South China Sea: implications for the tertiary tectonics of Southeast Asia. *J Geophys Res* 98:6299–6328
- Bullock AD, Minshull TA (2005) From continental extension to seafloor spreading: crustal structure of the Goban Spur rifted margin, southwest of the UK. *Geophys J Int* 163:527–546. doi:10.1111/j.1365-246X.2005.02726.x
- Chen S (1987) Magnetic profiles, in Atlas of Geology and Geophysics of the South China Sea, scale 1:2,000,000. Second Marine Geological Investigation Brigade of the Chinese Ministry of Geology and Mineral Resources, Guangdong
- Christensen NI, Mooney WD (1995) Seismic velocity structure and composition of the continental crust: A global view. *J Geophys Res* 100:9761–9788. doi:10.1029/95JB00259
- Chung S-L, Jahn B-M, Chen S-J, Lee T, Chen C-H (1995) Miocene basalts in northwestern Taiwan: evidence for EM-type mantle sources in the continental lithosphere. *Geochim Cosmochim Acta* 59:549–555
- Clift PD, Lin J, ODP Leg 184 Scientific Party (2001) Patterns of extension and magmatism along the continent-ocean boundary, South China margin. In: Wilson RCL, Beslier M-O, Whitmarsh RB, Froitzheim N, Taylor B (eds) Non-volcanic rifting of continental margins: a comparison of evidence from land and sea. Special Publications, vol 187. Geological Society of London, London, pp 489–510
- Dannowski A, Grevemeyer I, Ranero CR, Ceuleneer G, Maia M, Morgan JP, Gente P (2010) Seismic structure of an oceanic core complex at the Mid-Atlantic Ridge, 22°19'N. *J Geophys Res* 115:B07106. doi:10.1029/2009JB006943
- Dix C (1952) Seismic prospecting for oil. Harper and Brothers, New York
- Magnetic Anomaly Map of East Asia (1994) In Geological Survey of Japan and Committee for Co-ordination of Joint Prospecting for Mineral Resources in Asian offshore areas (CCOP)
- Gernigon L, Lucazeau F, Brigaud F, Ringenbach J-C, Planke S, Le Gall B (2006) A moderate melting model for the Vøring magin (Norway) based on structural observations and a thermo-kinematical modeling: Implication for the meaning of the lower crustal bodies. *Tectonophysics* 412:255–278
- Hsu S-K (2011) A new magnetic anomaly map in the surrounding area of Taiwan. 2011th continental shelf survey project of Taiwan report, Ministry of interior, Taiwan, 383 pp (in Chinese)
- Hsu S-K, Yeh Y-C, Doo W-B, Tsai C-H (2004) New bathymetry and magnetic lineations in the northernmost South China Sea and their tectonic implications. *Mar Geophys Res* 25:29–44. doi:10.1007/s11001-005-0731-7
- IAGA Working Group V-MOD (2010) The 11th-generation international geomagnetic reference field. *Geophys J Int* 183(3): 1216–1230. doi:10.1111/j.1365-246X.2010.04804.x
- Kido Y, Suyehiro K, Kinoshita H (2001) Rifting to spreading process along the Northern Continental Margin of the South China Sea. *Mar Geophys Res* 22:1–15. doi:10.1023/A:1004869628532
- Lester WR, McIntosh KD, Van Avendonk HJ (2010) Crustal-scale structure of the Eurasian Continental Margin in the Northern South China Sea, Offshore Taiwan from seismic reflection and wide-angle OBS data. Abstract T32C-07 presented at 2010 fall meeting, AGU, San Francisco, 13–17 Dec
- Li C-F, Zhou Z, Li J, Hao H, Geng J (2007) Structures of the northeasternmost South China Sea continental margin and ocean basin: geophysical constraints and tectonic implications. *Mar Geophys Res* 28:59–79. doi:10.1007/s11001-007-9014-9
- Lin AT, Watts AB, Hesselbo SP (2003) Cenozoic stratigraphy and subsidence history of the South China Sea margin in the Taiwan region. *Basin Res* 15(4):453–478
- Lin AT, Yao B, Hsu S-K, Liu C-S, Huang C-Y (2009) Tectonic features of the incipient arc-continent collision zone of Taiwan: implications for seismicity. *Tectonophysics* 479:28–42. doi:10.1016/j.tecto.2008.11.004
- Louden K, Chian D (1999) The deep structure of non-volcanic rifted continental margins. *Phil Trans R Soc Lond* 357:767–804
- Lüdmann T, Wong HK (1999) Neotectonic regime on the passive continental margin of the northern South China Sea. *Tectonophysics* 311:113–138
- Menzies MA, Klemperer SL, Ebinger CJ, Baker J (2002) Characteristics of volcanic margins. In: Menzies MA, Klemperer SL, Ebinger CJ, Baker J (eds) Volcanic rifted margins: Boulder, Colorado. Geological society of America special paper 362, pp 1–14
- Mjelde R, Kasahara J, Shinmamura H, Kamimura A, Kanazawa T, Kodaira S, Raum T, Shiobara H (2002) Lower crustal seismic velocity-anomalies; magmatic underplating or serpentinized peridotite? Evidence from the voring margin, NE Atlantic. *Mar Geophys Res* 23:169–183. doi:10.1023/A:1022480304527
- Nissen SS, Hayes DE, Buhl P, Diebold J, Yao B, Zeng W, Chen Y (1995) Deep penetration seismic soundings across the northern margin of the South China Sea. *J Geophys Res* 100:22407–22433
- Paige CC, Saunders MA (1982) LSQR: an algorithm for sparse equations and sparse least squares. *ACM Math Softw* 8:43–71
- Péron-Pinvidic G, Shillington DJ, Tucholke BE (2010) Characterization of sills associated with the U reflection on the Newfoundland margin: evidence for widespread early post-rift magmatism on a magma-poor rifted margin. *Geophys J Int* 182:113–136. doi:10.1111/j.1365-246X.2010.04635.x
- Ren J, Tamaki K, Li S, Junxia Z (2002) Late Mesozoic and Cenozoic rifting and its dynamic setting in Eastern China and adjacent areas. *Tectonophysics* 344:175–205. doi:10.1016/S0040-1951(01)00271-2

- Ru K, Pigott JD (1986) Episodic rifting and subsidence in the South China Sea. *Am Assoc Pet Geol Bull* 70(9):1136–1155
- Russell SM, Whitmarsh RB (2003) Magmatism at the West Iberia non-volcanic rifted continental margin; evidence from analyses of magnetic anomalies. *Geophys J Int* 154:706–730. doi:[10.1046/j.1365-246X.2003.01999.x](https://doi.org/10.1046/j.1365-246X.2003.01999.x)
- Sandwell DT, Smith WHF (1997) Marine gravity from Geosat and ERS 1 satellite altimetry. *J Geophys Res* 102:10039–10054. doi:[10.1029/96JB03223](https://doi.org/10.1029/96JB03223)
- Sibuet J-C, Tucholke B (2012) The geodynamic province of transitional crust adjacent to magma-poor continental margins. In: Mohriak W, Danfort A, Post P, Brown D, Tari G, Nemcock N, Sinha S (eds) *Divergent conjugate margins*. Geological Society of London, London (to submitted)
- Sibuet J-C, Hsu S-K, Le Pichon X, Le Formal J-P, Reed D, Moore GF, Liu C-S (2002) East Asia plate tectonics since 15 Ma: constraints from the Taiwan region. *Tectonophysics* 344:103–134. doi:[10.1016/S0040-1951\(01\)00202-5](https://doi.org/10.1016/S0040-1951(01)00202-5)
- Sibuet J-C, Srivastava S, Manatschal G (2007) Exhumed mantle-forming transitional crust in the Newfoundland-Iberia rift and associated magnetic anomalies. *J Geophys Res* 112:B06105. doi:[10.1029/2005JB003856](https://doi.org/10.1029/2005JB003856)
- Svensen H, Planke S, Malthe-Sorensen A, Jamtveit B, Myklebust R, Eidem T, Rey SS (2004) Release of methane from a volcanic basin as a mechanism for initial Eocene global warming. *Nature* 429:542–545
- Taylor B, Hayes DE (1980) The tectonic evolution of the South China Basin. In: Hayes DE (ed) *The tectonic and geologic evolution of Southeast Asian seas and islands*, vol 1. American Geophysics Union, Washington, pp 89–104
- Taylor B, Hayes DE (1983) Origin and history of the South China Sea basin. In: Hayes DE (ed) *The tectonic and geologic evolution of Southeast Asian Seas and Islands*, Part 2, *Geophys. Monogr. Ser.* AGU, Washington, pp 23–56
- Tsai C-H, Hsu S-K, Yeh Y-C, Lee C-S, Xia K-Y (2004) Crustal thinning of the northern continental margin of the South China Sea. *Mar Geophys Res* 25:63–78. doi:[10.1007/s11001-005-0733-5](https://doi.org/10.1007/s11001-005-0733-5)
- Tseng J-S (1994) Tertiary seismic sequence analysis of the Tainan basin. National Taiwan University master thesis, 102 pp in Chinese
- Tucholke BE, Sawyer DS, Sibuet J-C (2007) Breakup of the Newfoundland-Iberia rift margins. In: Karner GD, Manatschal G, Pinheiro LM (eds) *Imaging, mapping and modelling continental lithosphere extension and breakup*. Special Publications, vol 282. Geological Society of London, London pp 9–46. doi:[10.1144/SP282.2](https://doi.org/10.1144/SP282.2)
- Voss M, Jokat W (2007) Continent-ocean transition and voluminous magmatic underplating derived from P-wave velocity modeling of the East Greenland continental margin. *Geophys J Int* 170:580–604. doi:[10.1111/j.1365-246X.2007.03438.x](https://doi.org/10.1111/j.1365-246X.2007.03438.x)
- Wang T-K, Chen M-K, Lee C-S, Xia K (2006) Seismic imaging of the transitional crust across the northeastern margin of the South China Sea. *Tectonophysics* 412:237–254. doi:[10.1016/j.tecto.2005.10.039](https://doi.org/10.1016/j.tecto.2005.10.039)
- White RS, Smith LK (2009) Crustal structure of the Hatton and the conjugate east Greenland rifted volcanic continental margins, NE Atlantic. *J Geophys Res* 114:B02305. doi:[10.1029/2008JB005856](https://doi.org/10.1029/2008JB005856)
- White RS, McKenzie D, O’Nions K (1992) Oceanic crustal thickness from seismic measurements and rare earth element inversions. *J Geophys Res* 97:19683–19715. doi:[10.1029/92JB01749](https://doi.org/10.1029/92JB01749)
- White RS, Smith LK, Roberts AW, Christie PAF, Kusznir NJ, The rest of the iSIMM Team (2008) Lower-crustal intrusion on the North Atlantic continental margin. *Nature* 452:460–465. doi:[10.1038/nature06687](https://doi.org/10.1038/nature06687)
- Yeh Y-C, Hsu S-K (2004) Crustal structures of the northernmost South China Sea: seismic reflection and gravity modeling. *Mar Geophys Res* 25:45–61. doi:[10.1007/s11001-005-0732-6](https://doi.org/10.1007/s11001-005-0732-6)
- Yeh Y-C, Sibuet J-C, Hsu S-K, Liu C-S (2010) Tectonics evolution of the northeastern South China Sea from seismic interpretation. *J Geophys Res* 115:B06103. doi:[10.1029/2009JB006354](https://doi.org/10.1029/2009JB006354)
- Yen TP (1958) Cenozoic volcanic activity in Taiwan. *Taiwan Miner Ind* 10:1–39
- Yilmaz O (2008) *Seismic data analysis 2nd DVD version*. Society of Exploration Geophysics, Tulsa
- Zhao M, Qiu X, Xia S, Xu H, Wang P, Wang T-K, Lee C-S, Xia K (2010) Seismic structure in the northeastern South China Sea: S-wave velocity and Vp/Vs ratios derived from three-component OBS data. *Tectonophysics* 480(1–4):183–197. doi:[10.1016/j.tecto.2009.10.004](https://doi.org/10.1016/j.tecto.2009.10.004)